Journal of proteome research

Article

pubs.acs.org/jpr

Proteomic Analysis of Proteins Related to Prognosis of Lung Adenocarcinoma

Akiko Okayama,[†] Yohei Miyagi,[‡] Fumihiro Oshita,[‡] Mayuko Nishi,[§] Yoshiyasu Nakamura,[‡] Yoji Nagashima,[∥] Kazunori Akimoto,[⊥] Akihide Ryo,*[,§] and Hisashi Hirano*[,†]

[†]Graduate School of Medical Life Science and Advanced Medical Research Center, Yokohama City University, 3-9 Fukuura, Kanazawa-ku, Yokohama, Kanagawa 236-0004, Japan

[‡]Kanagawa Cancer Center, 2-3-2 Nakao, Asahi-ku, Yokohama, Kanagawa 241-8515, Japan

[§]Department of Microbiology and [∥]Department of Molecular Pathology, Yokohama City University Graduate School of Medicine, 3-9 Fukuura, Kanazawa-ku, Yokohama, Kanagawa 236-0004, Japan

[⊥]Department of Molecular Medical Science, Faculty of Pharmaceutical Sciences, Tokyo University of Science, 2641 Yamazaki, Noda, Chiba 278-8510, Japan

S *Supporting Information*

ABSTRACT: We attempted to identify prognosis-related proteins expressed in early resection lung adenocarcinomas that had higher metastatic potential. Early resection of lung adenocarcinoma tissues were collected from patients who experienced recurrence within 5 years after surgery; these patients are defined here as the poor prognosis group. From these samples, we prepared frozen tissue sections and then isolated cancerous areas by laser capture microdissection to allow extraction of cancer tissue-derived soluble proteins. Shotgun LC–MS/MS analysis detected and identified a total of 875 proteins in these cancer tissues. Relative quantitative analysis revealed that 17 proteins were preferentially expressed in the poor prognosis group relative to the good prognosis group, which consisted of patients who did not exhibit recurrence. Among them, 14-3-3 beta/alpha and calnexin were reported to be potentially involved in tumor recurrence and the malignant properties of lung cancer. Here immunological analyses confirmed disease-associated expression of these proteins. In a cell-culture model using A549, targeted depletion of either 14-3-3 beta/alpha or calnexin reduced proliferation, invasion, and migration, suggesting that both proteins are involved in determining the malignant properties of lung cancer that contribute to poor prognosis.

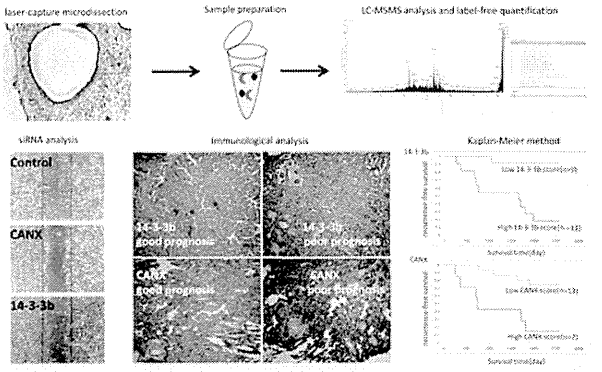

KEYWORDS: *lung adenocarcinoma, prognosis-related protein, shotgun LC–MS/MS analysis, label-free protein relative quantification, laser capture microdissection (LCM), 14-3-3 beta/alpha, calnexin*

INTRODUCTION

In recent years, favorable therapeutic outcomes have been achieved in many cases by detecting cancers in early stages, followed by surgical resection of the tumor. However, 20% of patients who undergo such early resection of lung adenocarcinoma exhibit recurrence and die within 5 years.[1,2] Therefore, treatments such as chemotherapy are often required in patients with stage I lung adenocarcinoma as well as those with stage II or III disease. However, such treatments are unnecessary for 80% of patients who undergo early resection.

Given this situation, there is an urgent need for biomarkers that allow diagnosis of patients with high risk of recurrence, who require various types of postoperative therapies. At the same time, it is essential to develop more effective post-operative adjuvant therapies. Previously, however, neither efficient nor effective techniques to identify such biomarker candidates were available.

Recently, proteomic approaches using sensitive and high-throughput technologies such as mass spectrometry have become powerful techniques for identifying potentially disease-associated proteins as biomarkers and therapeutic targets.[3,4] These techniques have made it possible to identify disease-associated proteins in small amounts of protein mixtures from tissues,[5] formalin-fixed paraffin-embedded tissues,[6] cultured cells,[7] and blood.[8] We hypothesized that we could use such techniques to identify biomarker candidates that allow diagnosis of patients with high risk of recurrence.

Special Issue: Proteomics of Human Diseases: Pathogenesis, Diagnosis, Prognosis, and Treatment

Received: December 27, 2013
Published: June 27, 2014

Recently, Ha et al.[9] performed two-dimensional electrophoresis (2-DE) on lung adenocarcinoma tissue proteins to detect proteins differentially expressed between patients with recurrence within 3 years and patients who remained disease-free for over 5 years by 2-DE. By mass spectrometry (MS/MS), they identified several proteins, including haptoglobin, annexin I, and serpin B6, as potential prognostic biomarkers. Similarly, Pernemaln et al.[10] analyzed primary lung adenocarcinoma tumor proteins by iTRAQ shotgun technique and identified proteins such as cathepsin D, ENO1, and VDAC1, which were related to the poor prognosis. Kikuchi et al.[11] analyzed proteins from two types of nonsmall cell lung cancer tissues and identified a total of 3621 proteins and cancer-specific proteins.

In this study, using techniques different from those used by Ha et al.,[9] Pernemalm et al.[10] and Kikuchi et al.,[11] we analyzed proteins that are differentially expressed between lung adenocarcinoma tissues from a poor prognosis group, in which patients exhibited recurrence within 5 years after surgery, and tissues from a good prognosis group, in which patients did not exhibit recurrence within 5 years after surgery. We used laser capture microdissection (LCM) to collect lung adenocarcinoma tissues and a shotgun LC–MS/MS technique to identify proteins associated with good or poor prognosis. Two of the proteins we identified, 14-3-3 beta/alpha and calnexin, were involved in proliferation, invasion, and migration of cancer cells. From these results, we concluded that these proteins might be prognosis-related protein lung cancer.

MATERIALS AND METHODS

Sample Preparation

Tissue samples extirpated from 21 patients at stage I (Ia or Ib) lung adenocarcinoma were obtained from the Kanagawa Cancer Center (Table 1). Tissues were collected only after receipt of informed consent from patients and kept at −80 °C until use.

Patients who exhibited recurrence within 5 years after extirpation were included in the poor prognosis group (8 patients), whereas patients who did not exhibit recurrence within 5 years after surgery were included in the good prognosis group (13 patients).

For LCM, each frozen tissue sample was sliced with a microtome (10 μm sections) and mounted on membrane-coated glass slides (2.0 μm thickness, 50 pieces, polyethylene naphthalate membrane; Leica, Milton Keynes, U.K.). Slides were kept at −80 °C and stained with Mayer's hematoxylin. From each section, ~2–6 mm^2 tissue areas containing defined stage I lung adenocarcinoma were dissected via LCM (Leica 6000, Leica).

Each frozen tissue sample was homogenized in 4 M urea, 2 M thiourea, and 1% (w/v) sodium deoxycholate containing Protease Inhibitor Mixture (GE Healthcare, Little Chalfont, U.K.) using a Sample Grinding Kit (GE Healthcare). Samples were then sonicated (Bioruptor UCD-250, Cosmo Bio, Tokyo, Japan) for 10 min and then reduced with 10 mM dithiothreitol and carbamidomethylated with 5 mM iodoacetamide at 37 °C for 60 min. The total amount of extracted protein was measured using the BCA protein assay kit–reducing agent compatible (Thermo Fisher Scientific, Bremen, Germany). Protein samples (3 μg each) were diluted four-fold with 500 mM triethylammonium bicarbonate at a final concentration of 1 M urea and then digested for 3 h at 37 °C with lysyl endprotease (Lys-C; Wako, Osaka, Japan) at a protein/enzyme ratio of 100:1 (w/w). Trypsin (Promega, Madison, MA) was added to the resultant peptide mixture sample at a protein/enzyme ratio of 20:1 (w/w), followed by incubation at 37 °C for 3 h. The same amount of trypsin was added a second time, and the sample was incubated at 37 °C overnight. Sodium deoxycholate was removed from the peptide solution by the phase-transfer surfactant (PTS) method;[12] then, samples were desalted using C18 stage tips.[13]

Table 1. Clinical and Pathological Data of Patients Whose Samples Were Subjected to LC–MS/MS Analysis and Western Blot Analysis[a]

sample no.	case	gender	age	TMN classification	tumor differentiation (G)
1077	good	female	71	T1N0M0	G1
126	good	male	57	T2N0M0	G3
128	good	male	74	T2N0M0	G3
220	good	male	71	T2N0M0	G3
391	good	female	56	T2N0M0	G2
429	good	female	70	T2N0M0	G2
446	good	female	39	T2N0M0	G1
533	good	male	79	T2N0M1	G2
385	good	male	69	T1N0M0	G1
858	good	male	74	T1N0M0	G1–G2
1016	good	female	70	T1N0M0	G1
1046	good	female	67	T2N0M1	G1–G2
1060	good	male	67	T1N0M0	
480	poor	male	66	T2N0M1	G3
365	poor	male	63	T1N1M0	G3
422	poor	female	65	T2N0M1	G3
472	poor	male	51	T2N0M1	G2
298	poor	female	68	T2N0M1	G2
322	poor	male	68	T1N0M0	G3
1105	poor	female	76	T1N0M1	G3
1006	poor	male	83	T2N0M1	G1

[a]Patients who exhibited recurrence within 5 years after extirpation were included in the poor prognosis group (8 patients), whereas patients who did not exhibit recurrence within 5 years after surgery were included in the good prognosis group (13 patients).

Shotgun LC–MS/MS Analysis

LC–MS/MS analysis was performed on a LTQ Orbitrap Velos (Thermo Fisher Scientific) using Xcalibur version 2.0.7 coupled to an UltiMate 3000 LC system (Dionex, LC Packings, Sunnyvale, CA).

Prior to injection into the mass spectrometer, trypsin-digested samples (1 μg each) were loaded online in a reverse-phase precolumn (C18 Pepmap column, LC Packings) and resolved on a nanoscale C18 Pepmap capillary column (75 μm i.d. × 15 cm) (LC Packings) with a gradient of acetonitrile/0.1% (v/v) formic acid at a flow rate of 300 nL/min. Peptides were separated using a 145 min gradient of 5–100% solvent B (0.1% [v/v] formic acid/95% [v/v] acetonitrile); solvent A was 0.1% (v/v) formic acid/2% (v/v) acetonitrile. Precursor ions were subject to dynamic exclusion for 180 s using a 5 ppm window and resolution of 60 000. Full-scan mass spectra were measured from 350–1200 m/z on an LTQ Orbitrap Velos mass spectrometer operated in data-dependent mode using the TOP10 strategy. MS/MS scanning conditions were as follows: normalized collision energy, 35.0%; isolation width, 2 m/z; activation time, 10 ms; activation Q, 0.25. The general mass spectrometric conditions were as follows: spray voltage, 2.1 kV; capillary temperature, 250 °C.

dx.doi.org/10.1021/pr4012969 | J. Proteome Res. 2014, 13, 4686–4694

Table 2. Clinical and Pathological Data of Patients Whose Samples Were Subjected to Immunohistochemical Analysis[a]

sample no.	case	gender	age	TNM classification	tumor differentiation (G)	survival time (day)	state
1	poor	female	72	T1aN0M0		259	lung cancer
2	poor	female	59	T1aN0M0	G3	365	lung cancer
3	poor	female	79	T1bN0M0		755	lung cancer
4	poor	male	56	T1bN0M0		675	lung cancer
5	poor	male	72	T1aN0M0	G3	707	lung cancer
6	poor	male	68	T1bN0M0	G1	1047	lung cancer
7	poor	female	58	T1aN0M0	G1	1672	lung cancer
8	poor	female	46	T1bN0M0	G1	1714	lung cancer
9	poor	female	75	T1bN0M0	G1	1811	lung cancer
10	poor	male	57	T1bN0M0	G2	1811	lung cancer
11	good	female	54	T1bN0M0	G1	2557	censoring
12	good	female	53	T1bN0M0	G1	2560	censoring
13	good	male	68	T1bN0M0	G1	2573	censoring
14	good	female	61	T1bN0M0	G1	2616	censoring
15	good	female	75	T1aN0M0	G1,G2	2625	censoring
16	good	male	56	T1aN0M0	G3	2410	censoring
17	good	male	78	T1bN0M0	G3	2414	censoring
18	good	female	53	T1bN0M0	G3	2556	censoring
19	good	female	59	T1aN0M0	G3	2557	censoring
20	good	male	71	T1bN0M0	G3	2621	censoring

[a]Patients who exhibited recurrence within 5 years after extirpation were included in the poor prognosis group (10 patients), whereas patients who did not exhibit recurrence within 5 years after surgery were included in the good prognosis group (10 patients).

Protein Identification and Label-Free Protein Relative Quantification

Label-free protein relative quantification was performed using the Progenesis LC–MS (v2.6, Nonlinear Dynamics, Durham, NC) data analysis software (Supplementary Figure S1 in the Supporting Information). Data generated by LC–MS/MS analysis of each amino-acid sequence and evaluated using Progenesis LC–MS were queried against the IPI_human database (December 18, 2009; 87 061 sequences) using Mascot (v2.3.02, Matrix Science, London, U.K.). The search parameters were as follows: trypsin digestion with two missed cleavages permitted; variable modifications, carbamidomethyl (C) and oxidation (M); peptide charge, 2+ or 3+; peptide mass tolerance for MS data, ± 5 ppm; fragment mass tolerance, ± 0.5 Da; score >30 and 5% false discovery rate (FDR). Proteins up-regulated in the poor prognosis group were extracted using the following parameters in Progenesis LC–MS: max fold change >1.5; $p < 0.05$ (one-way analysis of variance (ANOVA)); peptides used for quantification >3; difference between the minimum value in the poor prognosis group and maximum value in the good prognosis group >0.5 (to select proteins up-regulated in the poor prognosis group).

Western Blot Analysis

Proteins (each 10 μg) prepared by LCM according to the method described in the section of sample preparation were separated by SDS-PAGE using SuperSep Ace 12.5% 13-well gels (Wako Pure Chemical Industries) and then transferred to polyvinylidenedifluoride membranes using a Trans-Blot Turbo Transfer System (Bio-Rad Laboratories, Hercules, CA). Antimouse calnexin antibody (MBL, Nagoya, Japan), anti-rabbit 14-3-3 beta antibody (Immuno-Biological Laboratories, Gunma, Japan), and anti-mouse beta-actin antibody (Cell Signaling Technology, Danvers, MA) were used for western blot analysis. Membranes were incubated for 5 min with ECL Plus western blotting detection reagents (GE Healthcare). Protein signals were detected using a LAS 4000 mini luminescence image analyzer (GE Healthcare). The detected images were quantified using the ImageJ image processing and analysis software (v. 1.46, http://rsbweb.nih.gov/ij/index.html). We investigated using the one-way ANOVA to compare the significance of the between groups with of 14-3-3 beta/alpha and calnexin. Statistical tests were performed using GraphPad Prism 5 (V. 5.04, GraphPad Software, San Diego, CA).

Immunohistochemical Analysis

Ten samples for each prognosis group of stage I lung adenocarcinoma were formalin-fixed and paraffin-embedded after surgery (Table 2). Patients who exhibited recurrence within 5 years after extirpation were included in the poor prognosis group (10 patients), whereas patients who did not exhibit recurrence within 5 years after surgery were included in the good prognosis group (10 patients). Serial 4-μm sections of each specimen were examined by immunohistochemical analysis using anti–rabbit 14-3-3 beta antibody (1:300 dilution) (Chemicon, Billerica, MA) or antimouse calnexin antibody (1:100 dilution) (Chemicon). Antigen retrieval was performed by autoclaving at 121 °C for 15 min in 10 mM sodium citrate buffer (pH 6.0). Color development was performed using a fully automated immunohistostainer (Nichirei Biosciences, Tokyo, Japan) and the Histofine Simple Stain MAX-PO Kit (Nichirei Biosciences). In parallel, each sample was stained with 3,3′-diaminobenzine (DAB). To determine the fractional area stained with DAB, we calculated the average density per unit area using the color deconvolution function of ImageJ 1.46 (Color Deconvolution Function, http://www.mecourse.com/landinig/software/cdeconv/cdeconv.html).[14] It is possible to calculate the immunostain intensity of only the DAB. We investigated using one-way ANOVA to compare the significance of the between groups with of 14-3-3 beta/alpha and calnexin. We performed survival analysis (Kaplan–Meier method and log-rank test) to compare the DAB density of each protein between the good and poor prognosis groups.

Table 3. List of Proteins Identified As Up-Regulated in the Poor Prognosis Group Using the Progenesis LC–MS Data Analysis Software[a]

accession	protein name	max fold change	Anova (p)	score	peptide used for quantification	PPmin/ GPmax
IPI00913987	putative uncharacterized protein C18orf34	1.626	0.004	36	6	0.667
IPI00020984	calnexin	2.001	0.012	145	4	0.658
IPI00216318	isoform long of 14-3-3 protein beta/alpha	1.534	0.006	291	7	0.647
IPI00479786	KH-type splicing regulatory protein	1.531	0.020	123	7	0.637
IPI00916487	isoform 3 of catenin alpha-2	1.759	0.003	101	7	0.610
IPI00006865	vesicle-trafficking protein SEC22b	2.037	0.001	301	4	0.570
IPI00009960	isoform 1 of mitochondrial inner membrane protein	2.196	0.001	208	6	0.566
IPI00029012	eukaryotic translation initiation factor 3 subunit A	1.602	0.016	155	7	0.562
IPI00024284	basement membrane-specific heparan sulfate proteoglycan core protein	2.348	0.004	422	17	0.555
IPI00019884	alpha-actinin-2	1.813	0.002	160	4	0.548
IPI00893179	X-ray repair complementing defective repair in Chinese hamster cells 6	1.706	0.033	132	5	0.543
IPI00396485	elongation factor 1-alpha 1	1.507	0.005	410	8	0.534
IPI00007752	tubulin beta-2C chain	1.890	0.011	873	16	0.530
IPI00023598	tubulin beta-4 chain	1.885	0.014	780	14	0.525
IPI00382470	isoform 2 of heat shock protein HSP 90-alpha	1.649	0.041	819	16	0.515
IPI00152535	chromodomain-helicase-DNA-binding protein 5	1.666	0.033	81	5	0.511
IPI00167949	interferon-induced GTP-binding protein Mx1	1.730	0.012	128	5	0.501

[a]Conditions: max fold change >1.5; $p < 0.05$ (one-way ANOVA); peptides used for quantification >3; difference between the minimum value in the poor prognosis group and maximum value in the good prognosis group >0.5.

GraphPad Prism 5 (V. 5.04, GraphPad Software) was used for survival analysis.

Cell Culture

A549 cells (human alveolar adenocarcinoma cell line) were grown in Dulbecco's modified Eagle's medium (DMEM) (Nacalai Tesque, Kyoto, Japan) supplemented with 10% (w/v) fetal bovine serum, 100 units/mL penicillin, and 100 μg/mL streptomycin. The cells were cultured at 37 °C in a humidified atmosphere containing 5% CO_2.

Transfection of siRNA

A549 cells were transfected using HiPerFect (Qiagen, Valencia, CA). 14-3-3 beta/alpha and calnexin were silenced using custom-designed siRNAs (Hs_YWHAB_6 FlexiTube siRNA and CANX_6 FlexiTube siRNA, respectively; Qiagen). Control siRNA (sense strand, 5′-CAGUCGCGUUUGCGACUGGTT-3′; antisense strand, 5′-CCAGUCGCAAACGCGACUGTT-3′) was purchased from JBioS (Saitama, Japan). Cells were assayed 72 h after transfection.

Cell Invasion Assay

Cells were trypsinized and resuspended at 1×10^5 cells per 0.3 mL of serum-free media. Suspensions were added to the upper chambers of 24-well Transwell inserts (8 μm pore; BD Biosciences, Franklin Lakes, NJ) coated with 1 mg/mL Matrigel (BD Biosciences) dissolved in serum-free media. The bottoms of the wells were filled with 0.6 mL of serum-containing media containing 5 μg/mL fibronectin. After 24 h, the insets were removed, the upper surface of the filters were cleaned thoroughly with cotton swabs, and the lower surfaces were fixed for 10 min with 4% (v/v) paraformaldehyde (PFA) and subsequently stained for 5 min with 0.5% (w/v) crystal violet in 20% (v/v) methanol (upper chamber). Invasive cells were counted and scored in triplicate (lower chamber).

Wound-Healing Assay

Cell layers were gently wounded along the central axis of the plate using a pipet tip. Migration of cells into the wound was observed after 6 h in six randomly selected microscopic fields. Wound closures were quantitated using ImageJ 1.46.

RESULTS

LC–MS/MS Analysis and Label-Free Protein Relative Quantification

Using LCM, we collected <5 mm^2 of diseased areas of tissue samples from lung adenocarcinoma patients: 13 from the good prognosis group and 8 from the poor prognosis group. Minute quantities (in most cases, <15 μg) of protein were extracted from these areas. Next, the extracted protein samples were analyzed separately by LC–MS/MS, and proteins differentially expressed between the good and poor prognosis groups were identified by label-free relative protein quantitation using the Progenesis LC–MS software.

A total of 875 proteins were detected and identified in these samples. The complete list of identified proteins is shown in Supplementary Table S1 in the Supporting Information. We identified 17 proteins of which expression was higher in the poor prognosis group (Table 3).

Verification of Differentially Up-Regulated Proteins by Western Blot Analysis

We verified up-regulation of two of the identified proteins, 14-3-3 beta/alpha and calnexin, by western blot analysis (Figure 1a). The signal intensity of each band was quantitated by ImageJ 1.46 (Figure 1b). This analysis confirmed that 14-3-3 beta/alpha ($p < 0.005$) and calnexin ($p < 0.001$) were significantly up-regulated in the poor prognosis group (Figure 1b), suggesting that these proteins are related to prognosis of lung adenocarcinoma.

Immunohistochemical Validation of Up-Regulated Proteins in Poor Prognosis Lung Adenocarcinoma Tissues

We studied immunologically the aberrant expression of 14-3-3 beta/alpha and calnexin by microscopic imaging of tissue sections from patients in the good and poor prognosis groups

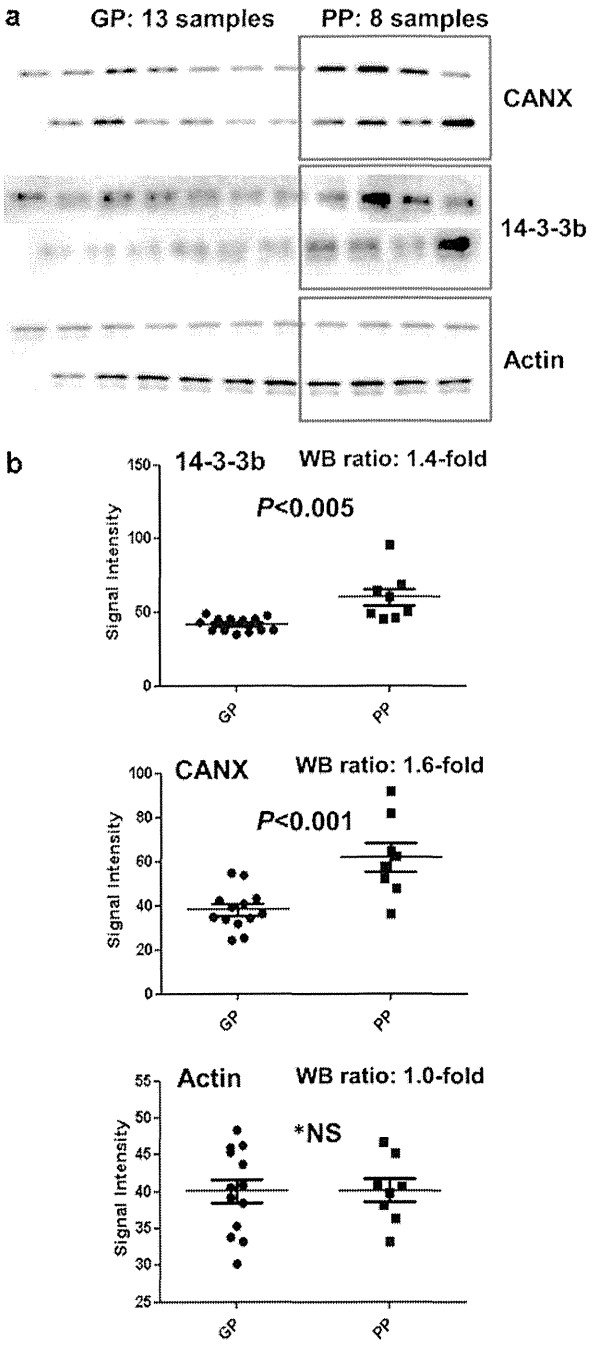

Figure 1. Validation of LC–MS/MS results. (a) Western blot analysis; GP, good prognosis group; PP, poor prognosis group; 14-3-3b, 14-3-3 beta/alpha; CANX, calnexin; actin, actin-beta as a control. (b) Western blot signal intensities quantitated using ImageJ 1.46. GP, good prognosis group; PP, poor prognosis group; 14-3-3b, 14-3-3 beta/alpha; CANX, calnexin. Western blot analysis ratio (WB ratio) = (average signal intensity of PP)/(average signal intensity of GP). *NS indicates no significance.

(10 patients each) (Figure 2a,b). The results also suggest that 14-3-3 beta/alpha and calnexin are related to prognosis of lung adenocarcinoma.

Next, we investigated the relationship between the expression levels of these two proteins and cancer recurrence using the Kaplan–Meier method and log-rank test to compare the significance of the recurrence-free curves between groups with high and low expression of 14-3-3 beta/alpha and calnexin. The results revealed a statistically significant difference ($p < 0.005$ and $p < 0.010$) in recurrence-free survival between the groups, indicating a strong association between expression of both proteins and tumor recurrence (Figure 2c).

14-3-3 Beta/Alpha and Calnexin Are Involved in Proliferation, Invasion, and Migration of Cancer Cells

We investigated the effects of 14-3-3 beta/alpha and calnexin on cancer cell growth, migration, and invasion. Initially, we investigated the expression of both proteins in four different lung adenocarcinoma cell lines (A549, HCC827, PC-3, and ABC-1). Immunoblot analysis revealed that both proteins were highly expressed in A549 cells, which are characterized by high migration and invasion capabilities (Figure 3a). To determine whether either or both proteins are involved in the malignant properties of these cells, we then attempted to suppress the expression of the two proteins in A549 cells by transfection with specific siRNAs. In conventional culture, cells transfected with siRNA against 14-3-3 beta/alpha and calnexin proliferated more slowly than cells transfected with control siRNA (Figure 3b).

Next, we investigated the effects of these siRNAs on the invasive and migratory abilities of A549 cells. Cells transfected with siRNA against 14-3-3 beta/alpha and calnexin exhibited significantly reduced invasive ability relative to control siRNA-treated cells (Figure 3c), suggesting that these proteins might be responsible for stimulating migration and invasion. Subsequently, using a wound-healing assay, we investigated whether migration of A549 cells was affected by knockdown of either 14-3-3 beta/alpha or calnexin. We observed distinctively slower wound healing, relative to control cells, in cells transfected with siRNAs against either protein (Figure 3d). Together, these results suggest that 14-3-3 beta/alpha and calnexin might play important roles in stimulating growth, migration, and invasion by human alveolar adenocarcinoma cells.

DISCUSSION

The goal of this study was to identify and validate proteins that are overexpressed in lung adenocarcinoma patients from a poor prognosis group, who exhibited recurrence or metastasis after early resection, and to suggest the suitability of these proteins as potential markers for prognosis prediction.

In the present study, only the diseased area was removed by LCM. The final amount of proteins extracted from this area was <15 μg. To analyze such minute quantities of protein, it was essential to combine LC–MS/MS analysis with subsequent label-free relative protein quantitation. Proteins were extracted from 13 lung adenocarcinoma patients from the good prognosis group and 8 patients from the poor prognosis group. The resultant samples were analyzed by LC–MS/MS, and proteins were differentially expressed between the two groups were by LC–MS/MS.

For this study, only a small number of clinical samples were available. However, we considered that even this small number was sufficient to show possibility to identify prognosis-related proteins. In the future, it will be necessary to conduct a large-scale study using a number of samples to use the proteins practically as biomarkers. Receiver operating characteristic (ROC) curves that we constructed as a trial using the data obtained in the present study are shown in Supplementary Figure S2 in the Supporting Information.

dx.doi.org/10.1021/pr4012969 | J. Proteome Res. 2014, 13, 4686–4694

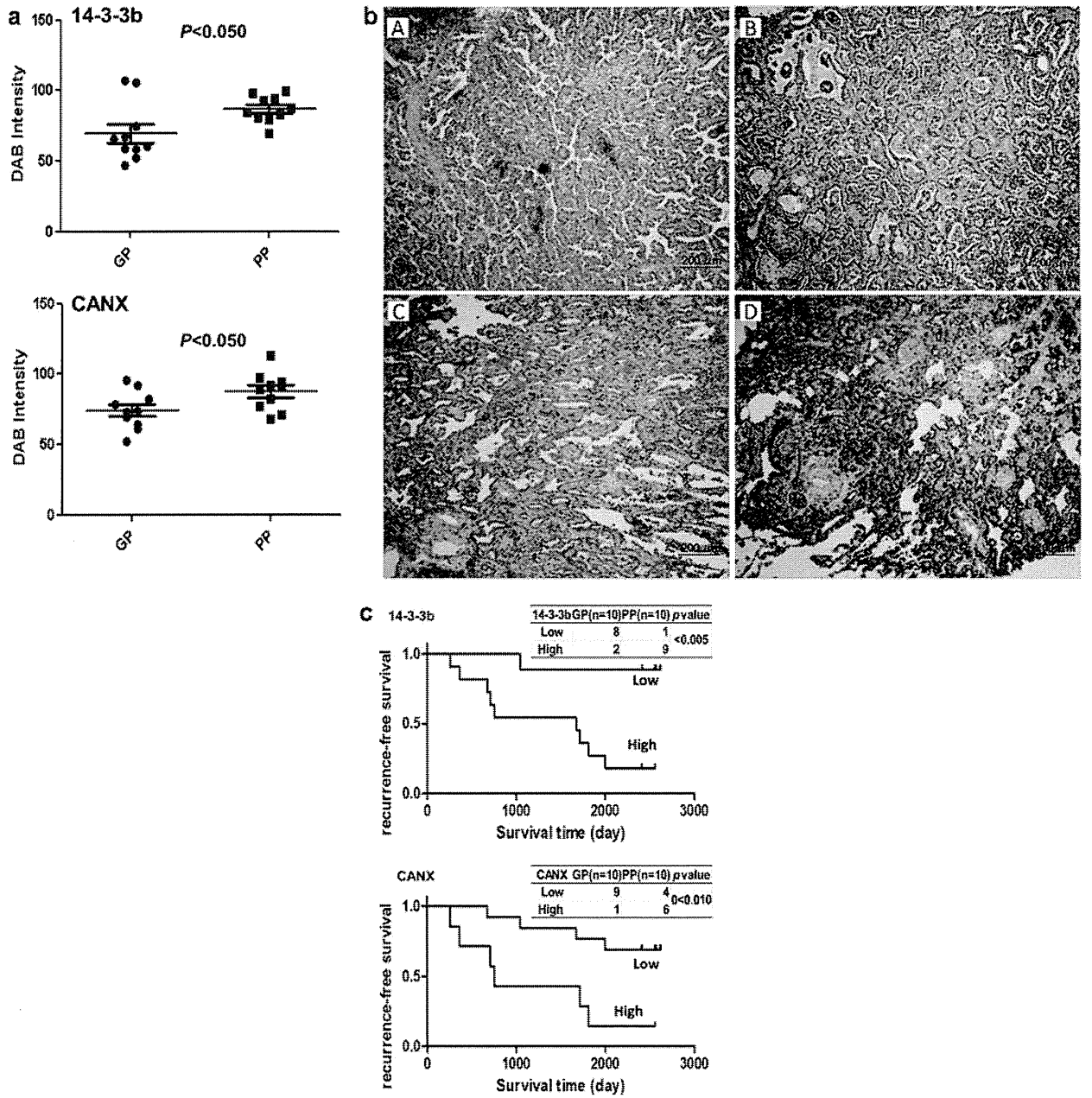

Figure 2. Validation of up-regulated proteins by immunohistochemistry. (a) Variance analysis was performed to calculate the average intensity of DAB in each sample. GP, good prognosis group; PP, poor prognosis group; 14-3-3b, 14-3-3 beta/alpha; CANX, calnexin. (b) Representative images of the mean intensity value in each group. All images are 400× magnification. Scale bars, 200 μm. Panels A and B show the average intensity of DAB staining for 14-3-3 beta/alpha. Panels C and D show the average intensity of DAB staining for calnexin. (A,C) Good prognosis group. (B,D) Poor prognosis group. 14-3-3 beta/alpha and calnexin were more strongly stained brown in panels B and D, respectively. (c) Two prognosis groups divided into lower-than-average and higher-than-average densities of DAB staining. Low expression of both proteins was associated with significantly higher survival. 14-3-3b, 14-3-3 beta/alpha; CANX, calnexin.

We collected and froze the tissue samples and preserved them for 5 years before performing proteomic analysis aimed at identifying prognosis-related proteins for lung adenocarcinoma. Among the 17 proteins overexpressed in the poor prognosis group, we selected two proteins previously uncharacterized in the context of relapse postsurgery in lung adenocarcinoma, 14-3-3 beta/alpha and calnexin. We also detected heat-shock protein 90 (HSP90) as a protein overexpressed in cancer with poor prognosis; a previous study indicated that inhibition of HSP90 affects cancer cell proliferation and survival.[15] In addition, we identified alpha-actinin and alpha-catenin using this approach. These proteins regulate cell adhesion and morphology, and their overexpression might be involved in cancer progression.[16,17] These results support the feasibility of our approach for identifying important proteins related to poor prognosis in cases of lung adenocarcinoma.

The results of the siRNA experiments in A549 cells suggested that 14-3-3 beta/alpha and calnexin are involved in growth, invasion, and migration of lung adenocarcinoma cells. Therefore, 14-3-3 beta/alpha and calnexin could be prognosis-related proteins for lung adenocarcinoma.

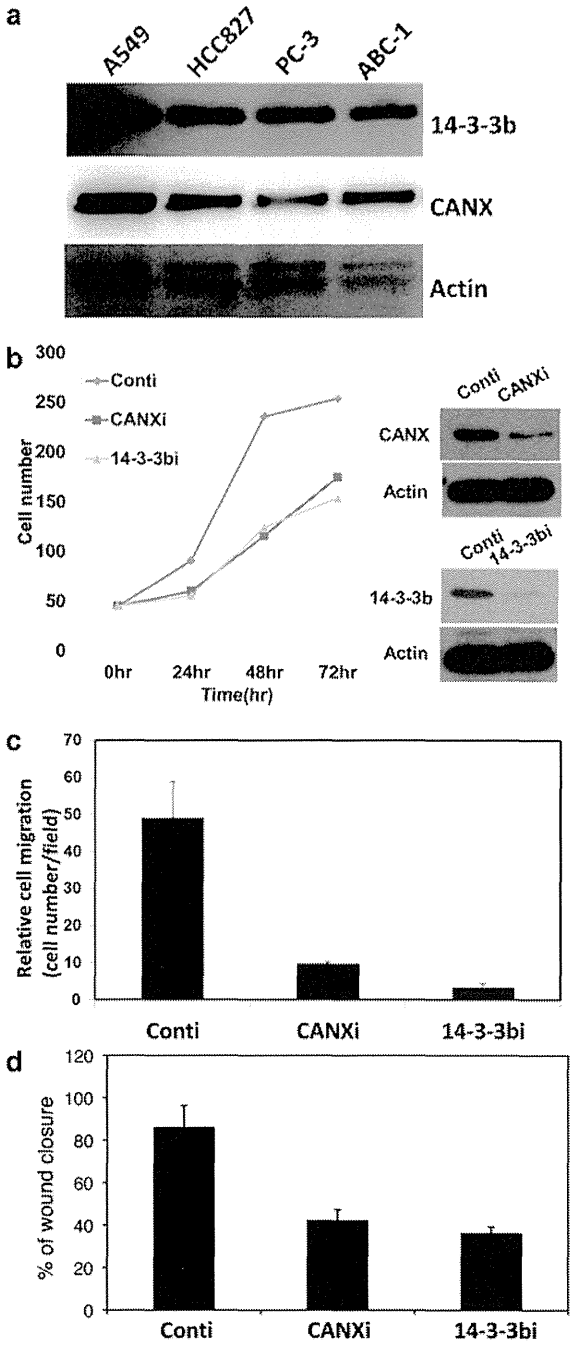

Figure 3. siRNA knockdown of 14-3-3 beta/alpha and calnexin confirms that these proteins influence proliferation, invasion, and migration. (a) Expression of each protein was examined by western blot analysis. 14-3-3b, 14-3-3 beta/alpha; CANX, calnexin; Cont, control; i, siRNA. (b) siRNA against 14-3-3b or CANX reduces growth in A549 cells. Cells were observed every 24 h. Expression of both proteins was confirmed by western blot analysis. 14-3-3b, 14-3-3 beta/alpha; CANX, calnexin; Cont, control; i, siRNA. (c) Migration assays were performed using chemotaxis chambers in transwell tissue-culture dishes (8 μm pore size). siRNA against 14-3-3b or CANX reduced migration by A549 cells. 14-3-3b, 14-3-3 beta/alpha; CANX, calnexin; Cont, control; i, siRNA. (d) Confluent layers of siRNA-transfected A549 or control cells were wounded with the tip of a pipet. siRNA against 14-3-3b or CANX reduced growth and invasion by A549 cells. 14-3-3b, 14-3-3 beta/alpha; CANX, calnexin; Cont, control; i, siRNA.

The 14-3-3 proteins are phosphoserine/phosphothreonine-binding proteins that control the activities of target proteins, thereby regulating cellular functions such as signal transduction, cell growth, differentiation, the cell cycle, and cell motility.[18−22] Proteins of the 14-3-3 family reside primarily in the cytoplasm, although some members are bound to the cell membrane, endoplasmic reticulum (ER) membrane, or Golgi membrane; interactions between 14 and 3-3 proteins and oncoproteins localized to the cell membrane suggest that 14-3-3 proteins are involved in oncogenesis.[19]

14-3-3 beta, gamma, sigma, and theta are expressed at elevated levels in lung cancer tissue, and these isoforms might be involved in the onset of lung tumors.[23] Moreover, several previous reports have demonstrated that the 14-3-3 protein family is also involved in the epithelial-to-mesenchymal transition (EMT) and may thereby contribute to the progress of cancer.[24] Furthermore, 14-3-3 family proteins promote tumorigenicity and angiogenesis in hepatocellular carcinoma.[25]

Calnexin is involved in ensuring proper protein folding in the ER,[26] where many membrane-bound and secreted proteins are synthesized. The ER facilitates both protein folding and degradation of misfolded proteins.[27,28] Accumulation of misfolded proteins in this compartment results in ER stress, which promotes tumor progression[29] as well as the pathogenesis of Alzheimer's disease and Parkinson's disease.[28,30,31] The expression level of calnexin can directly influence tunicamycin sensitivity and ER stress-mediated apoptosis in MCF-7 breast cancer cells.[32] A better understanding of the roles of chaperones in protein folding may clarify the mechanisms underlying these diseases and facilitate the development of new treatments.

Ha et al.[9] identified proteins differentially expressed between patients with recurrence within 3 years and those that were disease-free for over 5 years. They identified completely different proteins from those that we detected. In their study, they used 2-DE to detect these proteins and identified by MS/MS, but they did not use LCM to collect the adenocarcinoma tissues as samples. We used this method to precisely collect adenocarcinoma tissues and then used shotgun techniques instead of 2-DE/MS/MS to detect and identify the proteins. This difference in experimental strategy might explain why the two studies identified nonoverlapping sets of proteins.

Similarly, Pernemalm et al.[10] identified proteins related to patients with recurrence within 2 years of surgery by iTRAQ MS/MS shotgun method. They described in detail about cathepsin D, ENO1, and VDAC1 in their paper. They also found that calnexin was up-regulated in the poor prognosis group. This is the same result as ours. Although they did not validate this protein in detail, we confirmed, based on their result, that this protein was related to the prognosis.

Kikuchi et al.[11] compared protein profiles between two subtypes of nonsmall cell lung cancer and normal tissues by shotgun analysis. They identified a total of 3621 proteins and differentially expressed proteins such as calcitonin-related polypeptide alpha, carbamoil-phosphate synthase 1, and chromogranin B between lung adenocarcinoma and normal tissues. Kikuchi et al.[11] also detected 14-3-3 zeta/delta belonging to the same protein family as 14-3-3 beta/alpha. However, they did not recognize that this protein was a prognosis-related protein.

We detected up-regulation of C18orf34 in the poor prognosis lung adenocarcinoma. However, we did not validate this protein because the anti-C18orf34 antibody was not

commercially available for its validation, and we failed to amplify mRNA coding for C18orf34 by PCR. Therefore, in the present study, we focused on 14-3-3 beta/alpha and calnexin.

The proteomic approach described here, in which we used stored samples, could be useful for the identification of prognosis-related proteins for lung adenocarcinoma. We expect that our study sheds light on the prognostic prediction of early resection lung adenocarcinomas.

■ ASSOCIATED CONTENT

Supporting Information

Supplementary Table S1: List of the identified proteins. Supplementary Figure S1: Three-dimensional views show specific peptides from 14 to 3-3 beta/alpha (14-3-3b) and calnexin (CANX) from single samples from the good prognosis group (GP) and poor prognosis group (PP). Peptide peaks were extracted using the Progenesis LC–MS software, which integrates the intensity of each detected ion to calculate peak volume. These views show the peak volumes from the LC–MS data and also the isotopic patterns of the eluting peptides. Supplementary Figure S2: ROC curve analyses of the ability of 14-3-3 beta/alpha (14-3-3b) and calnexin (CANX) to discriminate patients between good and poor prognosis groups. This material is available free of charge via the Internet at http://pubs.acs.org.

■ AUTHOR INFORMATION

Corresponding Authors

*A.R.: Tel: +81-45-2600. Fax: +81-45-787-2851. E-mail: aryo@yokohama-cu.ac.jp.
*H.H.: Tel: +81-45-787-2993. Fax: +81-45-787-2787. E-mail: hirano@yokohama-cu.ac.jp.

Notes

The authors declare no competing financial interest.

■ ACKNOWLEDGMENTS

This work was partially supported by Special Coordination Funds for Promoting Science and Technology "Creation of Innovation Centers for Advanced Interdisciplinary Research Areas" in "Project for Developing Innovation Systems".

■ REFERENCES

(1) Naruke, T.; Tsuchiya, R.; Kondo, H.; Asamura, H. Prognosis and survival after resection for bronchogenic carcinoma based on the 1997 TNM-staging classification: the Japanese experience. *Ann. Thorac. Surg.* **2001**, *71*, 1759–1764.

(2) Kondo, T.; Yamada, K.; Noda, K.; Nakayama, H.; Kameda, Y. Radiologic-prognostic correlation in patients with small pulmonary adenocarcinomas. *Lung Cancer* **2002**, *36*, 49–57.

(3) Qian, W. J.; Jacobs, J. M.; Liu, T.; Camp, D. G., 2nd; Smith, R. D. Advances and challenges in liquid chromatography-mass spectrometry-based proteomics profiling for clinical applications. *Mol. Cell. Proteomics.* **2006**, *5*, 1727–1744.

(4) Makarov, A.; Denisov, E.; Kholomeev, A.; Balschun, W.; Lange, O.; Strupat, K.; Horning, S. Performance evaluation of a hybrid linear ion trap/orbitrap mass spectrometer. *Anal. Chem.* **2006**, *78*, 2113–2120.

(5) Kuramitsu, Y.; Nakamura, K. Proteomic analysis of cancer tissues: shedding light on carcinogenesis and possible biomarkers. *Proteomics* **2006**, *6*, 5650–5661.

(6) Hood, B. L.; Darfler, M. M.; Guiel, T. G.; Furusato, B.; Lucas, D. A.; Ringeisen, B. R.; Sesterhenn, I. A.; Conrads, T. P.; Veenstra, T. D.; Krizman, D. B. Proteomic analysis of formalin-fixed prostate cancer tissue. *Mol. Cell. Proteomics.* **2005**, *4*, 1741–1753.

(7) Keshamouni, V. G.; Michailidis, G.; Grasso, C. S.; Anthwal, S.; Strahler, J. R.; Walker, A.; Arenberg, D. A.; Reddy, R. C.; Akulapalli, S.; Thannickal, V. J.; Standiford, T. J.; Andrews, P. C.; Omenn, G. S. Differential protein expression profiling by iTRAQ-2DLC-MS/MS of lung cancer cells undergoing epithelial-mesenchymal transition reveals a migratory/invasive phenotype. *J. Proteome Res.* **2006**, *5*, 1143–1154.

(8) Tanaka, Y.; Akiyama, H.; Kuroda, T.; Jung, G.; Tanahashi, K.; Sugaya, H.; Utsumi, J.; Kawasaki, H.; Hirano, H. A novel approach and protocol for discovering extremely low-abundance proteins in serum. *Proteomics* **2006**, *6*, 4845–4855.

(9) Ha, E. S.; Choi, S.; In, K. H.; Lee, S. H.; Lee, E. J.; Lee, S. Y.; Kim, J. H.; Shin, C.; Shim, J. J.; Kang, K. H.; Phark, S.; Sul, D. Identification of proteins expressed differently among surgically resected stage I lung adenocarcinomas. *Clin. Biochem.* **2013**, *46* (4–5), 369–377.

(10) Pernemalm, M.; De Petris, L.; Branca, R. M.; Forshed, J.; Kanter, L.; Soria, J. C.; Girard, P.; Validire, P.; Pawitan, Y.; van den Oord, J.; Lazar, V.; Påhlman, S.; Lewensohn, R.; Lehtiö, J. Quantitative proteomics profiling of primary lung adenocarcinoma tumors reveals functional perturbations in tumor metabolism. *J. Proteome Res.* **2013**, *12* (9), 3934–3943.

(11) Kikuchi, T.; Hassanein, M.; Amann, J. M.; Liu, Q.; Slebos, R. J.; Rahman, S. M.; Kaufman, J. M.; Zhang, X.; Hoeksema, M. D.; Harris, B. K.; Li, M.; Shyr, Y.; Gonzalez, A. L.; Zimmerman, L. J.; Liebler, D. C.; Massion, P. P.; Carbone, D. P. In-depth proteomic analysis of nonsmall cell lung cancer to discover molecular targets and candidate biomarkers. *Mol. Cell Proteomics.* **2012**, *11* (10), 916–932.

(12) Masuda, T.; Tomita, M.; Ishihama, Y. Phase transfer surfactant-aided trypsin digestion for membrane proteome analysis. *J. Proteome Res.* **2008**, *7*, 731–740.

(13) Rappsilber, J.; Mann, M.; Ishihama, Y. Protocol for micro-purification, enrichment, pre-fractionation and storage of peptides for proteomics using StageTips. *Nat. Protoc.* **2007**, *2*, 1896–1906.

(14) Safadi, R. A.; Musleh, A. S.; Al-Khateeb, T. H.; Hamasha, A. A. Analysis of immunohistochemical expression of k19 in oral epithelial dysplasia and oral squamous cell carcinoma using color deconvolution-image analysis method. *Head Neck Pathol.* **2010**, *4*, 282–289.

(15) Jhaveri, K.; Miller, K.; Rosen, L.; Schneider, B.; Chap, L.; Hannah, A.; Zhong, Z.; Ma, W.; Hudis, C.; Modi, S. A phase I dose-escalation trial of trastuzumab and alvespimycin hydrochloride (KOS-1022; 17 DMAG) in the treatment of advanced solid tumors. *Clin. Cancer Res.* **2012**, *18*, 5090–5098.

(16) Knudsen, K. A.; Soler, A. P.; Johnson, K. R.; Wheelock, M. J. Interaction of alpha-actinin with the cadherin/catenin cell-cell adhesion complex via alpha-catenin. *J. Cell Biol.* **1995**, *130*, 67–77.

(17) Watabe-Uchida, M.; Uchida, N.; Imamura, Y.; Nagafuchi, A.; Fujimoto, K.; Uemura, T.; Vermeulen, S.; van Roy, F.; Adamson, E. D.; Takeichi, M. alpha-Catenin-vinculin interaction functions to organize the apical junctional complex in epithelial cells. *J. Cell Biol.* **1998**, *142*, 847–857.

(18) Conklin, D. S.; Galaktionov, K.; Beach, D. 14–3-3 proteins associate with cdc25 phosphatases. *Proc. Natl. Acad. Sci. U. S. A.* **1995**, *92*, 7892–7896.

(19) Freeman, A. K.; Morrison, D. K. 14–3-3 Proteins: diverse functions in cell proliferation and cancer progression. *Semin Cell Dev Biol.* **2011**, *22*, 681–687.

(20) Reuther, G. W.; Fu, H.; Cripe, L. D.; Collier, R. J.; Pendergast, A. M. Association of the protein kinases c-Bcr and Bcr-Abl with proteins of the 14–3-3 family. *Science.* **1994**, *266*, 129–133.

(21) Pallas, D. C.; Fu, H.; Haehnel, L. C.; Weller, W.; Collier, R. J.; Roberts, T. M. Association of polyomavirus middle tumor antigen with 14–3-3 proteins. *Science.* **1994**, *265*, 535–537.

(22) Bonnefoy-Bérard, N.; Liu, Y. C.; von Willebrand, M.; Sung, A.; Elly, C.; Mustelin, T.; Yoshida, H.; Ishizaka, K.; Altman, A. Inhibition of phosphatidylinositol 3-kinase activity by association with 14–3-3 proteins in T cells. *Proc. Natl. Acad. Sci. U. S. A.* **1995**, *92*, 10142–10146.

(23) Qi, W.; Liu, X.; Qiao, D.; Martinez, J. D. Isoform-specific expression of 14–3-3 proteins in human lung cancer tissues. *Int. J. Cancer.* **2005**, *113*, 359–363.
(24) Hou, Z.; Peng, H.; White, D. E.; Wang, P.; Lieberman, P. M.; Halazonetis, T.; Rauscher, F. J., 3rd. 14-3-3 binding sites in the snail protein are essential for snail-mediated transcriptional repression and epithelial-mesenchymal differentiation. *Cancer Res.* **2010**, *70*, 4385–4393.
(25) Komiya, Y.; Kurabe, N.; Katagiri, K.; Ogawa, M.; Sugiyama, A.; Kawasaki, Y.; Tashiro, F. A novel binding factor of 14–3-3beta functions as a transcriptional repressor and promotes anchorage-independent growth, tumorigenicity, and metastasis. *J. Biol. Chem.* **2008**, *283*, 18753–18764.
(26) Hammond, C.; Braakman, I.; Helenius, A. Role of N-linked oligosaccharide recognition, glucose trimming, and calnexin in glycoprotein folding and quality control. *Proc. Natl. Acad. Sci. U. S. A.* **1994**, *91*, 913–917.
(27) Ellgaard, L.; Helenius, A. Quality control in the endoplasmic reticulum. *Nat. Rev. Mol. Cell Biol.* **2003**, *4*, 181–191.
(28) Wickner, S.; Maurizi, M. R.; Gottesman, S. Posttranslational quality control: folding, refolding, and degrading proteins. *Science.* **1999**, *286*, 1888–1893.
(29) Mahadevan, N. R.; Rodvold, J.; Sepulveda, H.; Rossi, S.; Drew, A. F.; Zanetti, M. Transmission of endoplasmic reticulum stress and pro-inflammation from tumor cells to myeloid cells. *Proc. Natl. Acad. Sci. U. S. A.* **2011**, *108*, 6561–6566.
(30) Wickner, S.; Maurizi, M. R.; Gottesman, S. Posttranslational quality control: folding, refolding, and degrading proteins. *Science* **1999**, *286*, 1888–1893.
(31) Hashimoto, M.; Rockenstein, E.; Crews, L.; Masliah, E. Role of protein aggregation in mitochondrial dysfunction and neurodegeneration in Alzheimer's and Parkinson's diseases. *NeuroMol. Med.* **2003**, *4*, 21–36.
(32) Delom, F.; Emadali, A.; Cocolakis, E.; Lebrun, J. J.; Nantel, A.; Chevet, E. Calnexin-dependent regulation of tunicamycin-induced apoptosis in breast carcinoma MCF-7 cells. *Cell Death Differ.* **2007**, *14*, 586–596.

Alternative Mammalian Target of Rapamycin (mTOR) Signal Activation in Sorafenib-resistant Hepatocellular Carcinoma Cells Revealed by Array-based Pathway Profiling*[S]

Mari Masuda‡§, Wei-Yu Chen¶, Akihiko Miyanaga‡, Yuka Nakamura‡, Kumiko Kawasaki‖, Tomohiro Sakuma‖, Masaya Ono‡, Chi-Long Chen¶, Kazufumi Honda‡, and Tesshi Yamada‡

Sorafenib is a multi-kinase inhibitor that has been proven effective for the treatment of unresectable hepatocellular carcinoma (HCC). However, its precise mechanisms of action and resistance have not been well established. We have developed high-density fluorescence reverse-phase protein arrays and used them to determine the status of 180 phosphorylation sites of signaling molecules in the 120 pathways registered in the NCI-Nature curated database in 23 HCC cell lines. Among the 180 signaling nodes, we found that the level of ribosomal protein S6 phosphorylated at serine residue 235/236 (p-RPS6 S235/236) was most significantly correlated with the resistance of HCC cells to sorafenib. The high expression of p-RPS6 S235/236 was confirmed immunohistochemically in biopsy samples obtained from HCC patients who responded poorly to sorafenib. Sorafenib-resistant HCC cells showed constitutive activation of the mammalian target of rapamycin (mTOR) pathway, but whole-exon sequencing of kinase genes revealed no evident alteration in the pathway. p-RPS6 S235/236 is a potential biomarker that predicts unresponsiveness of HCC to sorafenib. The use of mTOR inhibitors may be considered for the treatment of such tumors. ***Molecular & Cellular Proteomics 13: 10.1074/mcp.M113.033845, 1429–1438, 2014.***

Hepatocellular carcinoma (HCC)[1] is the third most common cause of cancer-related death worldwide (1). Advanced HCC often cannot be managed with local treatments (surgical resection, ethanol injection, radiofrequency ablation, chemoembolization), but no systemic chemotherapy with conventional cytotoxic agents had been shown to be effective until a landmark phase III clinical trial (the Sorafenib HCC Assessment Randomized Protocol) revealed significant survival prolongation in patients treated with sorafenib (Nexavar; Bayer Healthcare Pharmaceuticals Inc. Berlin, Germany) (2). Furthermore, it has been reported that some patients show remarkable tumor shrinkage after short-term administration of sorafenib (3). Based on these results, sorafenib monotherapy has been employed as the current standard first-line treatment for unresectable HCC. However, not all HCC patients show the desired therapeutic benefits of sorafenib. The overall survival prolongation of unselected patients in the SHARP trial was limited to 2.8 months (2), and an objective tumor response was observed only in a small proportion of patients (0.6% to 2%) (2, 4). Given the relatively high cost and occasional severe adverse events (diarrhea, hand-foot skin reaction, hypertension, and others) (2, 4), there is an urgent need to identify a predictive biomarker that could exclude advanced HCC patients who are unlikely to benefit from sorafenib therapy.

Sorafenib is a multi-kinase inhibitor that blocks tumor cell proliferation and angiogenesis through the inhibition of c-RAF and b-RAF, as well as many receptor tyrosine kinases, including vascular endothelial growth factor receptors 2 and 3, platelet-derived growth factor receptor-α, Fms-related tyrosine kinase 3, RET, and c-KIT (5). In view of this broad inhibitory spectrum, the precise mechanisms underlying the anti-

From the ‡Division of Chemotherapy and Clinical Research, National Cancer Center Research Institute, Tokyo, 104-0045 Japan; ¶Department of Pathology, Wan Fan Hospital and Taipei Medical University, Taipei, 11031 Taiwan; ‖BioBusiness Group, Mitsui Knowledge Industry, Tokyo, 164-8555 Japan

Received August 23, 2013, and in revised form, February 2, 2014
Published, MCP Papers in Press, March 18, 2014, DOI 10.1074/mcp.M113.033845

Author contributions: M.M. and T.Y. designed research; M.M., W.C., A.M., and Y.N. performed research; M.M. and K.K. contributed new reagents or analytic tools; M.M., W.C., K.K., T.S., and C.C. analyzed data; M.M. and T.Y. wrote the paper; M.M. developed the methodology; M.O. and K.H. contributed to the conception of the study; T.Y. supervised research.

[1] The abbreviations used are: HCC, hepatocellular carcinoma; ERK, extracellular signal-regulated kinase; IC_{50}, half-maximal (50%) inhibitory concentration; p-RPS6 S235/236, ribosomal protein S6 phosphorylated at the serine 235/236 residue; MAPK, mitogen-activated protein kinase; RPPA, reverse-phase protein array; mTOR, mammalian target of rapamycin; RSK, 90-kDa ribosomal protein S6 kinase; S6K, 70-kDa ribosomal protein S6 kinase.

tumor activity remain elusive. To date, factors that have been identified as correlated with the efficacy of sorafenib include phosphorylated extracellular signal-regulated kinase 1 (p-ERK) (6), serum des-γ-carboxyprothrombin level (7), phosphorylated c-Jun protein (8), and fibroblast growth factor-3/4 gene amplification (3), but their clinical utility as predictive biomarkers has not been established.

In the present study, we developed a new technique, high-density fluorescence reverse-phase protein array (RPPA), and used it to search for a biomarker that would identify patients in whom sorafenib would be effective, employing a large library of phosphorylation-site-specific antibodies. RPPA represents an emerging technology for proteomics, and it is well suited for the profiling of phosphorylated proteins. It involves micro-format dot immunoblotting of lysates from tissues or cells (9), allowing simultaneous monitoring of the expression of a particular phosphoprotein in hundreds to thousands of samples under identical conditions in a highly quantitative manner (10). In this study we profiled the activation status of 180 key signaling nodes across a panel of 23 HCC cell lines and identified *de novo* activation of mTOR signaling in sorafenib-resistant HCC cells.

EXPERIMENTAL PROCEDURES

Cell Lines and Antibodies—Cell lines used for generating the cancer cell line RPPA are listed in supplemental Table S1 and were maintained according to their suppliers' recommendations. Recombinant EGF was obtained from R&D Systems (Minneapolis, MN). A total of 180 phosphorylation-site-specific antibodies and their dilutions used for RPPA analysis are listed in supplemental Table S2. The specificity of each antibody was verified by immunoblotting or had been previously described by other investigators.

RPPA—Cells were collected by scraping and stored at −80°C until use. Cell lysates were prepared with RIPA buffer (Thermo Scientific, Rockford, IL) supplemented with phosphatase (Thermo Scientific) and protease (Sigma, St. Louis, MO) inhibitor cocktails. Protein concentrations of lysates were determined via the Bradford method (Bio-Rad Laboratories, Hercules, CA). The lysates were serially diluted 2-fold four times and printed in quadruplicate onto ProteoChip glass slides (Proteogen, Seoul, South Korea) using a robotic spotter (Genex Arrayer, Kaken Geneqs Inc., Chiba, Japan).

The RPPA slides were incubated overnight with primary antibodies. Following tyramide signal amplification (Dako Cytomation, Glostrup, Denmark), streptavidin Alexa Fluor 647 conjugate (Invitrogen, Carlsbad, CA) was applied to the slides (11). Fluorescence images were captured by an InnoScan 700 microarray scanner (Innopsys, Carbonne, France) and quantified using Mapix software (Innopsys). After background subtraction, values relative to γ-tubulin were subjected to quantile normalization (12) to ensure a uniform distribution of values for each slide in a set of slides. Unsupervised hierarchical clustering, using the Euclidean metric and Ward's method, was conducted with R 2.13.0. The signaling components of the mTOR and MAPK pathways were selected based on KEGG pathway maps and used for clustering analyses.

Immunoblot Analysis—Immunoblot analyses were performed using the NuPAGE Bis-Tris or Tris-Acetate electrophoresis system (Invitrogen) as described previously (13). All antibodies except for an anti-p-RSK (S380) antibody (R&D Systems) were obtained from Cell Signaling Technology (Danvers, MA). Signals were detected with the ImageQuant LAS 4010 system (GE Healthcare, Giles, UK) and quantified using the ImageQuant TL software package (GE Healthcare).

Growth Inhibition Assay—Sorafenib, RAD001 (everolimus), and SL0101 were purchased from Toronto Research Chemicals Inc. (North York, Ontario, Canada). CI-1040 and AZD8055 were from Selleck Chemicals (Houston, TX). Stock solutions of the chemicals were prepared in dimethyl sulfoxide and stored at −20°C until use. Cells were seeded into 96-well cell culture plates in triplicate at a density of 3000 cells per well. On the following day, serially diluted drugs were added, and 72 h later cell viability was measured using the CellTiter-Glo Luminescent Cell Viability Assay (Promega, Fitchburg, WI). Relative cell viability was calculated as a percentage of a control treated with 0.1% dimethyl sulfoxide after background subtraction. All experiments were repeated at least three times. The data were modeled using a four-parameter log-logistic nonlinear regression curve fit with a sigmoid dose response. These curves were drawn using R 2.13.0, and IC_{50} values were calculated accordingly.

Immunohistochemistry—Formalin-fixed, paraffin-embedded sections of needle biopsy samples obtained from nine HCC patients before administration of sorafenib at Wan Fang Hospital and the Taipei Medical University Hospital were immunostained with anti-p-RPS6 Ser235/236 (#2211, Cell Signaling Technology) or anti-RPS6 (#2217, Cell Signaling Technology) antibody, as described previously (13). The stained slides were evaluated by pathologists and classified according to the percentage of positively stained cells (0 = 0%, 1 = 1% to 25%, 2 = 26% to 50%, 3 = 51% to 75%, and 4 = 76% to 100%) and the intensity of staining (0, absent; 1, weak; 2, moderate; and 3, strong). A specimen was defined as positive when either the percentage of positively stained cells or the intensity of staining was 3 or higher. The use of clinical materials was approved by the respective institutional review boards.

Kinome Sequencing—Genomic DNA was extracted from 20 HCC cell lines using the DNeasy Blood and Tissue kit (Qiagen, Hilden, Germany), in accordance with the manufacturer's protocol. DNA concentration was determined using a NanoDrop 2000 spectrophotometer (Thermo Scientific). Three micrograms of genomic DNA was used to construct libraries for sequencing. The quality of the constructed libraries was assessed using an Agilent 2100 Bioanalyzer (Agilent Technologies, Santa Clara, CA). All the exon and 5′- and 3′-flanking sequences (200 bp) of 511 kinase genes were captured using a customized SureSelect Target Enrichment System (Agilent Technologies) according to the Illumina Paired-End Sequencing Platform Library Prep Protocol Version 1.0 (Agilent Technologies). Captured DNA fragments (~300 bp) were sequenced using a Genome Analyzer IIx sequencer (Illumina, San Diego, CA). Base calling was performed using the Illumina Pipeline (v1.4) with default parameters. Only paired end (2 × 75 bases) sequence reads that passed the quality control were mapped to the human reference genome build hg19 (UCSC hg19) using BWA (14) with default parameters. Sequencing artifacts were eliminated using Picard MarkDuplicates. Variants were called with SAMtools (15) and annotated using Annovar ENREF 25 (16). The final set of novel variant calls was identified using the following thresholds: SNP quality ≥ 228, coverage ≥ 20 reads, frequency ≥ 10%, and not deposited in the dbSNP database (www.ncbi.nlm.nih.gov/projects/SNP/) (version 135).

Evaluation of Synergistic Drug Combinations—The synergistic interaction of drug combinations was evaluated using the Chou–Talalay median-dose effect method (17) with CompuSyn software. AZD8055 and CI-1040 were mixed at the ratio of their IC_{50} values (1:300). The mixed solution was 2-fold serially diluted five times and added to the cells. Combination Index values were calculated at the points causing 50%, 75%, and 90% reduction of cell viability. Combination Index values equal to 1, >1, and <1 indicate additive, antagonistic, and synergistic interactions, respectively.

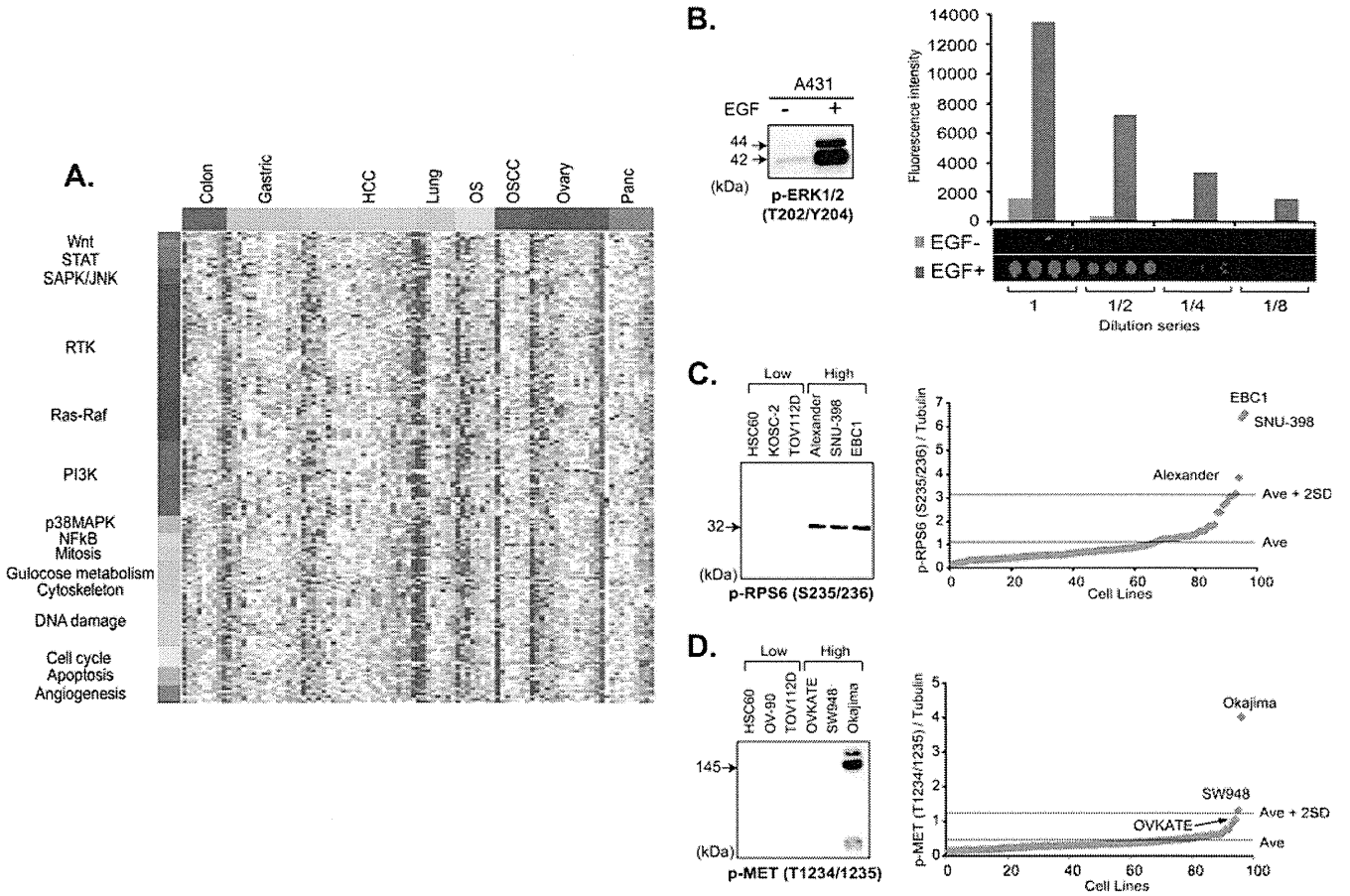

FIG. 1. **Phosphoprofiling of key signaling molecules by RPPA.** *A*, phosphorylation status of 180 signaling nodes in a panel of 95 cancer cell lines cultured in the presence of 10% FCS. Red and blue colors indicate high- and low-level phosphorylation, respectively. STAT, signal transducers and activators of transcription; SAPK/JNK, stress-activated protein kinase/c-Jun NH_2-terminal kinase; RTK, receptor tyrosine kinase; PI3K, phosphatidylinositol 3′-kinase; MAPK, mitogen-activated protein kinase; NFκB, nuclear factor-kappaB; OS, osteosarcoma; OSCC, oral squamous cell carcinoma. *B*, immunoblot (*left*) and RPPA (*right*) analyses of A431 cells cultured without (−) and with (+) EGF for 10 min with anti-p-ERK1/2 (T202/Y204) antibody. The mean fluorescence intensity in arbitrary units (*top*) and images (*bottom*) of quadruplicate RPPA spots of lysate undiluted (1) and diluted 1:2 (1/2), 1:4 (1/4), and 1:8 (1/8) -fold are shown (*right*). *C*, *D*, relative p-RPS6 S235/236 (*C*) and p-Met T1234/1235 (*D*) expression of 95 cell lines determined via RPPA (right). Cell lines with the three highest and three lowest levels of expression were selected and subjected to immunoblotting with the same antibody (*left*). Ave, average.

RESULTS

Generation of the High-density RPPA and Phosphoprotein Profiling—We constructed an RPPA onto which lysates of 95 cell lines derived from eight different types of cancer (listed in supplemental Table S1) cultured in the presence and absence of 10% fetal calf serum (FCS) for 17 h and A431 cells untreated or treated with 200 ng/ml EGF for 10 min were randomly plotted. Each lysate was serially diluted (1:1, 1:2, 1:4, and 1:8) and spotted in quadruplicate (16 spots per lysate). This level of high-density spotting (3072 samples per array slide) was achievable because of the highly hydrophobic surface of the array slides, which prevented diffusion of the protein samples.

By applying 180 phosphorylation-site-specific antibodies (listed in supplemental Table S2), we determined the activation status of signaling proteins (Fig. 1*A*). A lysate of A431 cells treated with EGF was included as a positive internal control. A431 cells carry amplification of the *EGFR* (EGF receptor) gene. We confirmed that a >6-fold increase in the signal intensity of ERK1/2 proteins phosphorylated at the threonine 202/tyrosine 204 residue (p-ERK1/2 T202/Y204) was detectable after treatment with EGF (Fig. 1*B*).

To further verify the data obtained via RPPA, lysates of representative cell lines were electrophoresed and blotted with the same antibodies. In the RPPA analysis, EBC1, SNU-398, and Alexander cells showed a high signal intensity for anti-p-RPS6 S235/236 antibody, exceeding the average plus 2 S.D. for 96 cell lines, whereas TOV112D, KOSC-2, and HSC60 cells showed a signal intensity below the average (Fig. 1*C*, right). The results we obtained from immunoblotting were consistent (Fig. 1*C*, left).

The glass slides that we used for construction of the RPPA were free of any autofluorescence noise. The use of fluorescent dyes and original signal enhancement significantly in-

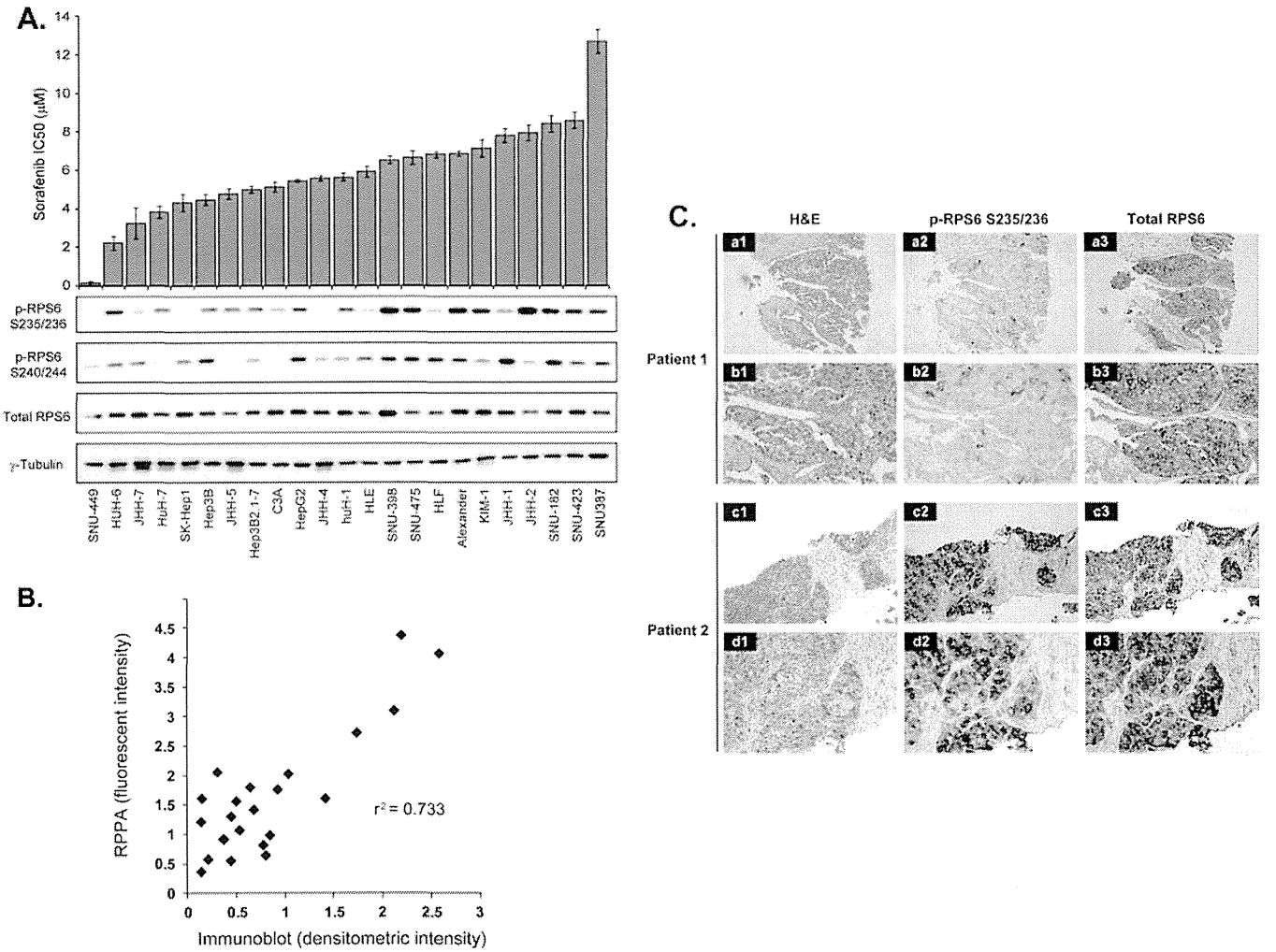

FIG. 2. **p-RPS6 S235/236 correlates with the sensitivity of HCC to sorafenib.** *A*, *upper graph*, IC_{50} values for sorafenib against 23 HCC cell lines sorted from the most sensitive (*left*) to resistant (*right*) ones. Columns and error bars represent the mean and S.D. of three independent experiments, respectively. *Lower panels*, immunoblot analysis of pRPS6 S235/236, pRPS6 S240/244, RPS6, and γ-tubulin (loading control) expression in the 23 HCC cell lines. *B*, correlation between RPPA and immunoblot analyses of p-RPS6 S235/236 expression in the 23 HCC cell lines (R^2 = 0.733). *C*, detection of p-RPS6 S235/236 in pretreatment biopsy samples. Hematoxylin and eosin (H&E) (a-d1) and immunoperoxidase staining with anti-p-RPS6 S235/236 (a-d2) and total RPS6 (a-d3) antibodies of HCC biopsy specimens obtained from a responder (patient 1 (a and b)) and a representative non-responder (patient 2 (c and d)) to sorafenib. Original magnification was ×40 (a1–3 and c1–3) and ×200 (b1–3 and d1–3).

creased the sensitivity of signal detection. In fact, MET protein with a high level of phosphorylation (p-MET T1234/1235) in Okajima cells was detectable via immunoblotting, whereas the MET protein with a relatively low level of phosphorylation in SW948 and OVKATE cells was undetectable (Fig. 1*D*).

p-RPS6 S235/236 Correlates with the Sensitivity of HCC Cells to Sorafenib—The cancer cell protein array contained 23 HCC cell lines exhibiting a wide variety of sensitivities to sorafenib (Fig. 2*A*, upper portion). SNU-449 was the most sensitive, with a half-maximal (50%) inhibitory concentration (IC_{50}) of 0.172 μM. It was ~70-fold more sensitive than the least sensitive cell line, SNU-387 (IC_{50} = 12.68 μM). We then compared the IC_{50} value of each HCC cell line with the phosphorylation level of 180 signaling nodes. Spearman's correlation coefficient analysis (supplemental Table S3) revealed that p-RPS6 S235/236 had the highest positive correlation (r = 0.58, p = 0.0044), followed by p-RPS6 at the serine 240/244 residues (p-RPS6 S240/244) (r = 0.55, p = 0.0070). 90-kDa ribosomal S6 kinase 2 (RSK2) protein phosphorylated at the serine 227 residue showed the third most significant correlation. RSK2 is one of the enzymes that phosphorylate RPS6 (18).

Consistent with the RPPA data, intense signals for p-RPS6 S235/236 were detected in the sorafenib-resistant cell lines via immunoblotting (Fig. 2*A*, lower portion). The quantified immunoblot data correlated well with those of RPPA (r^2 = 0.733), thus confirming the precision of the RPPA (Fig. 2*B*). p-RPS6 S235/236 and p-RPS6 S240/244 exhibited different

phosphorylation patterns among several cell lines (*e.g.* HLF, KIM1, JHH-1, and JHH-2) (Fig. 2*A*, lower portion), suggesting that phosphorylation of S235/236 and S240/244 residues may be mediated by distinct regulatory processes.

p-RPS6 S235/236 Is a Potential Predictor of Response to Sorafenib—We next evaluated whether high levels of p-RPS6 S235/236 were indicative of HCC resistance to sorafenib in clinical samples (supplemental Table S4). Expression of p-RPS6 S235/236 was examined in biopsy specimens collected from nine HCC patients prior to sorafenib treatment (400 mg twice a day). Eight patients showed intense staining for p-RPS6 (Fig. 2*C*). Four patients (Cases 4, 6, 7, and 9) with p-RPS6-positive tumors discontinued sorafenib treatment because of disease progression within 2.3 months. Four patients (Cases 2, 3, 5, and 8) died as a result of disease progression after starting sorafenib treatment. In contrast, the remaining patient (Case 1), whose tumor was negative for p-RPS6, received sorafenib for 24 months and survived for 27 months. In this particular patient, tumor regression was confirmed by computed tomography scans performed three months after sorafenib administration and remained stable for another three months. In addition, the α-fetoprotein level dropped from 1621 to 314 ng/ml and remained low for 10 months. These results provide preliminary evidence that that high expression of p-RPS6 S235/236 might be useful for predicting which patients are unlikely to respond to sorafenib. As biopsy is not performed routinely before sorafenib treatment, we were unable to further validate the clinical significance of p-RPS6 S235/236 by examining additional cases.

mTOR Pathway Activation in Sorafenib-resistant Cells—Given the association between p-RPS6 and sensitivity of HCC cell lines to sorafenib, we assessed the effects of sorafenib on p-RPS6 in representative sorafenib-sensitive and -resistant cell lines. The sorafenib-sensitive HUH-6 and HuH-7 cell lines demonstrated substantial dose-dependent decreases in p-RPS6 levels following treatment with sorafenib (Fig. 3*A*). Sorafenib also diminished the phosphorylation of downstream molecules in the MAPK pathway, ERK and RSK, in a dose-dependent manner (Fig. 3*A*), implying that the reduction of p-RPS6 in sorafenib-sensitive cells was likely attributable to blockade of the MAPK pathway (Fig. 3*B*).

In contrast, the phosphorylation of RPS6 S235/236 in sorafenib-resistant cell lines, especially JHH-2, SNU-423, and SNU-387 cells, was insensitive to the same sorafenib treatment (Fig. 3*C*). The level of p-RPS6 in JHH-1 and SNU-182 cells decreased to some extent after sorafenib treatment, but a high concentration (10 μM) of sorafenib was necessary in order to suppress the phosphorylation of RPS6 completely (Fig. 3*C*), reflecting that the regulation of p-RPS6 in sorafenib-resistant cell lines is different from that in sensitive cell lines. RPS6 is also known to be phosphorylated by 70-kDa ribosomal S6 kinases (S6K) downstream of mTOR (Fig. 3*B*) (19, 20). We therefore speculated that the mTOR pathway might be alternatively activated in sorafenib-resistant cell lines. In fact, we found that sorafenib-resistant cells had a high level of p-S6K1 (Fig. 3*C*), whereas p-S6K1 was barely detectable in sorafenib-sensitive cells (Fig. 3*A*).

The phosphorylation of ERK in JHH-1 and SNU-182 was suppressed to some extent by sorafenib, but the low level of p-RSK and high level of p-S6K1 indicate that the main regulator of RPS6 phosphorylation was mTOR signaling rather than MAPK signaling.

Absence of Genetic Alterations in the MAPK and mTOR Pathways—RAF kinases are among the known targets of sorafenib, but sorafenib-resistant JHH2, SNU-423, and SNU-387 cells exhibited sustained activation of molecules located downstream of RAF (ERK and RSK), even in the presence of sorafenib (Fig. 3*C*), suggesting sorafenib-insensitive activation of the MAPK pathway.

To clarify the molecular mechanism driving the activation of the mTOR and MAPK pathways in sorafenib-resistant cells, we sequenced the entire exons of 511 kinases (listed in supplemental Table S5) in 20 HCC cell lines using a next-generation sequencer. Supplemental Table S6 lists all of the 322 genetic alterations that were not deposited in the dbSNP database. Due to the unavailability of normal counterparts, we were unable to determine whether these alterations were somatic. Eight kinds of DNA alterations were evident in the known mTOR and MAPK pathway genes (Supplemental Table S7). b-RAF V600E, found in SK-Hep1 cells, is a known driver mutation frequently observed in malignant melanoma (21). Two kinds of alterations were identified in the ATP-binding (S72A (JHH-7)) and AGC-kinase C-terminal (K335T (huH-1, SNU-475, and SNU-185)) domains of the RSK1 genes. Three kinds of alterations were found in the proline-rich domain (A420V (11 cell lines including SNU449) and V422I (HUH-6)) and catalytic (P267L (SK-Hep1, JHH-4, Kim1, and JHH-1)) domains of the S6K2 gene.

These eight alterations were validated using a conventional sequencing method (Supplemental Table S7), but no genetic alteration was specific to sorafenib-resistant cell lines. Infrequent alteration of the mTOR and MAPK pathway genes in HCC has been demonstrated by conventional sequencing analysis of surgical samples (22), and this was consistent with the present comprehensive sequencing data. The aberrant activation of the mTOR and MAPK pathways in sorafenib-resistant HCC cells was likely attributable to complex interplay between other oncogenic and anti-oncogenic pathways, or post-translational modifications.

mTOR Inhibitors Repress the Proliferation of Sorafenib-resistant Cells—The marked inhibition of p-RPS6 S235/236 following exposure to an mTOR inhibitor, everolimus, at a concentration as low as 2 nM (Fig. 3*D*) confirmed that activation of the mTOR pathway is responsible for the sorafenib-insensitive phosphorylation of RPS6 S235/236 in sorafenib-resistant cells. Consistently, sorafenib-insensitive cells tended to be more sensitive to another mTOR inhibitor,

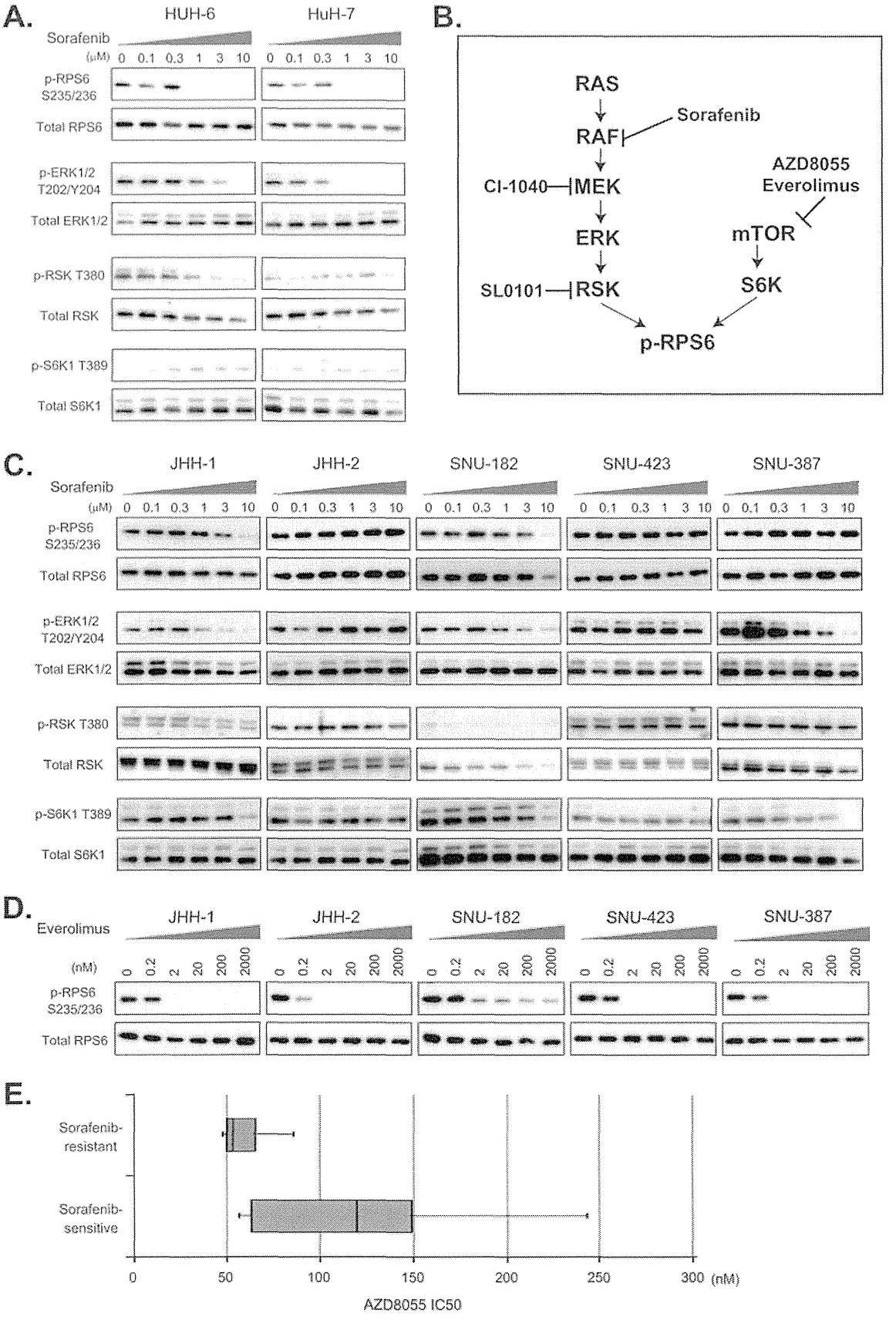
A.
HUH-6
HuH-7
Sorafenib
(μM) 0 0.1 0.3 1 3 10 0 0.1 0.3 1 3 10
p-RPS6 S235/236
Total RPS6
p-ERK1/2 T202/Y204
Total ERK1/2
p-RSK T380
Total RSK
p-S6K1 T389
Total S6K1
B.
RAS
RAF
Sorafenib
CI-1040
MEK
AZD8055
Everolimus
ERK
mTOR
SL0101
RSK
S6K
p-RPS6
C.
JHH-1
JHH-2
SNU-182
SNU-423
SNU-387
Sorafenib
(μM) 0 0.1 0.3 1 3 10
p-RPS6 S235/236
Total RPS6
p-ERK1/2 T202/Y204
Total ERK1/2
p-RSK T380
Total RSK
p-S6K1 T389
Total S6K1
D.
Everolimus
(nM) 0 0.2 2 20 200 2000
p-RPS6 S235/236
Total RPS6
E.
Sorafenib-resistant
Sorafenib-sensitive
0 50 100 150 200 250 300 (nM)
AZD8055 IC50

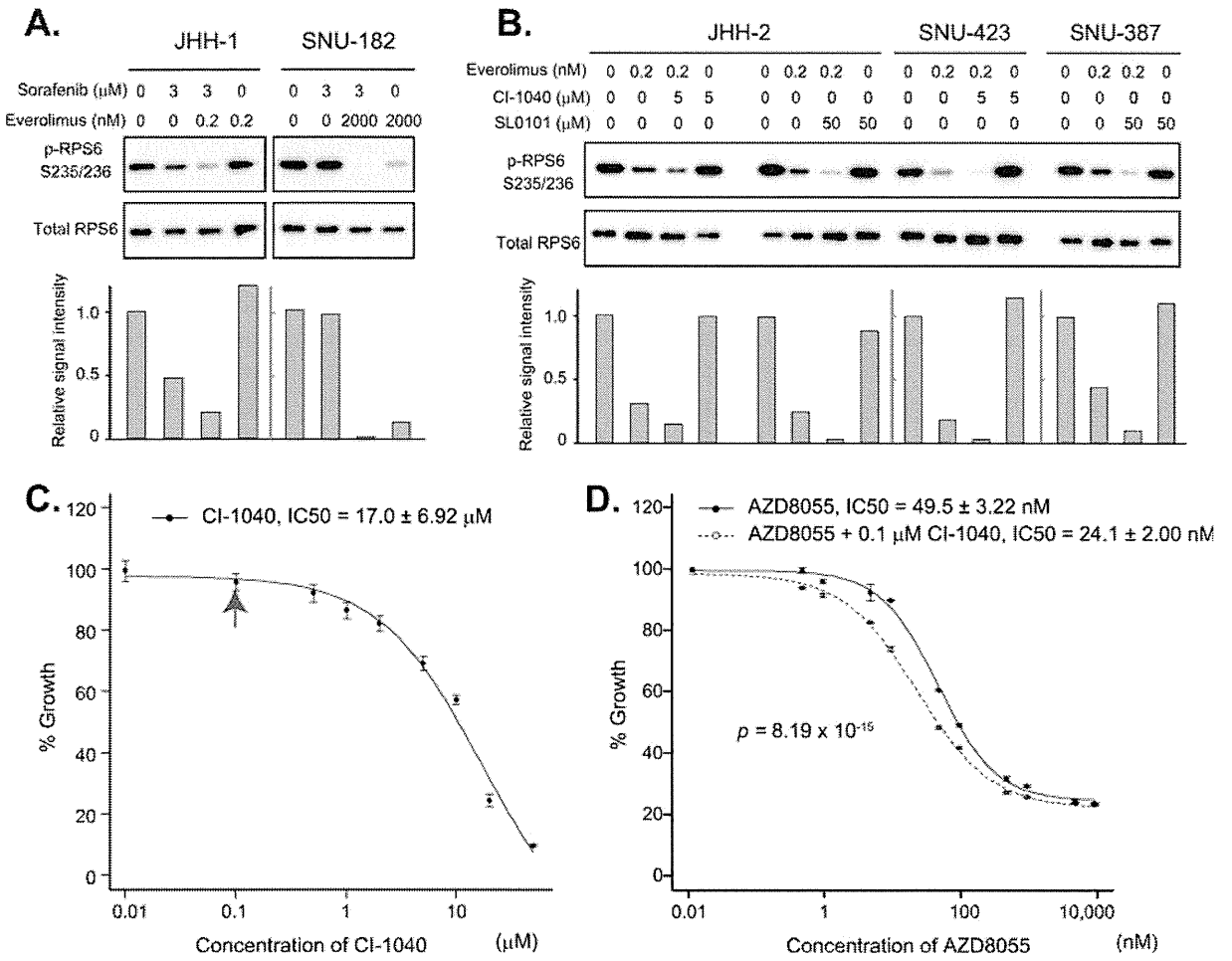

FIG. 4. **Synergy of mTOR and MAPK inhibitors.** *A*, sorafenib-resistant JHH-1 and SNU-182 cells were treated with the indicated concentrations of sorafenib and everolimus, and the expression of p-RPS6 S235/236 and total RPS6 was examined via immunoblotting (*top*). The bottom panel indicates intensity relative to control blots (no treatment). *B*, sorafenib-resistant JHH2, SNU-423 and SNU-387 cells were treated with the indicated concentrations of CI-1040, SL0101, and everolimus, and the expression of p-RPS6 S235/236 and RPS6 was examined via immunoblotting (*top*). The bottom panel indicates blot intensities relative to control blots (no drug treatment). *C*, sorafenib-resistant SNU-423 cells were treated with the indicated concentrations of CI-1040, and relative cell viability was determined 72 h later. Note that CI-1040 had no significant inhibitory effect on cell growth at 0.1 μM (indicated by a red arrow). *D*, sorafenib-resistant SNU-423 cells were treated with the indicated concentrations of AZD8055 in the presence (open circles) or absence (solid circles) of 0.1 μM CI-1040, and relative cell viability was determined 72 h later.

AZD8055, than sorafenib-sensitive cell lines (Fig. 3*E*), indicating that sorafenib-resistant cells are dependent for growth on constitutive activation of the mTOR pathway.

Synergy of mTOR and MAPK Inhibitors—Although JHH-1 and SNU-182 cells showed resistance to sorafenib, their ERK phosphorylation was dose-dependently attenuated by sorafenib (Fig. 3*C*), indicating that the MAPK pathway in these cells still retained some sensitivity to the inhibition of RAF or other unknown MAPK-pathway kinases. In fact, sorafenib augmented the down-regulation of p-RPS6 S235/236 by everolimus (Fig. 4*A*). It is noteworthy that the low level of p-RPS6 S235/236 in SNU-182 cells sustained in the presence of 2 μM everolimus was completely abrogated by the addition of 3 μM sorafenib.

FIG. 3. **Alternative mTOR signal activation in sorafenib-resistant HCC cells.** *A*, *C*, representative sorafenib-sensitive (HUH-6 and HuH-7) and -resistant (JHH-1, JHH-2, SNU-182, SNU423, and SNU-387) HCC cells were treated with the indicated concentrations of sorafenib for 3 h, and the expression of p-RPS6 S235/236, total RPS6, p-ERK1/2 T202/Y204, total ERK, p-RSK T380, total RSK, p-S6K T389, and total S6K was determined via immunoblotting. *B*, schematic representation of the mTOR and MAPK pathways and their inhibitors. *D*, representative sorafenib-resistant (JHH-1, JHH-2, SNU-182, SNU423, and SNU-387) HCC cells were treated with the indicated concentrations of everolimus for 3 h, and the expression of p-RPS6 S235/236 and total RPS6 was determined via immunoblotting. *E*, distribution of IC_{50} values of representative sorafenib-sensitive (SNU-449, HUH-6, JHH-7, HuH-7, and SK-Hep1) and -resistant (JHH-1, JHH-2, SNU-182, SNU-423, and SNU-387) HCC cells to AZ8055. Boxes indicate 25th to 75th percentiles.

The phosphorylation of RPS6 S235/236 in JHH-2, SNU-423, and SNU-387 cells was insensitive to sorafenib (Fig. 3*C*). However, the active MAPK pathway in these cell lines seems to lie downstream of RAF kinases. An MEK inhibitor, CI-1040 (Fig. 3*B*), enhanced the attenuation of p-RPS6 S235/236 by everolimus in JHH-2 and SNU-423 cells (Fig. 4*B*), and an RSK inhibitor, SL0101, enhanced the attenuation of p-RPS6 S235/236 by everolimus in JHH-2 and SNU-387 cells (Fig. 4*B*).

Marked inhibition of p-RPS6 S235/236 by combined blockade of the MAPK pathway downstream of RAF and the mTOR pathway prompted us to examine the effect of this drug combination on HCC cell growth. CI-1040 had no inhibitory effect on the growth of SNU-423 cells at a concentration of 0.1 μM (Fig. 4*C*), but it was able to enhance the growth-inhibitory effect of AZD8055 (Fig. 4*D*). Synergy between AZD8055 and CI-1040 was confirmed via Chou–Talalay median dose effect analysis (17) (supplemental Table S8). The combination index values at 50%, 75%, and 90% growth inhibition were 0.783, 0.804, and 0.827, respectively (values of <1 are defined as representative of synergistic effects). These results suggest that HCC patients refractory to sorafenib with a high level of p-RPS6 S235/236 might be treatable with an mTOR inhibitor in combination with drugs that block the MAPK signaling pathway.

To further provide a rational basis for synergistic targeting of the mTOR and MAPK pathways in HCC, we performed unsupervised hierarchical cluster analysis of 23 HCC cell lines based on their phosphorylation status of signaling components in the mTOR and MAPK pathways listed in supplemental Table S9. Clustering analysis stratified the cell lines into two major groups, A and B (supplemental Fig. S1). In comparison with group A, group B showed higher levels of phosphorylated MAPK signaling components including p-PDGF receptor-β(Thr751), p-Raf-A(Ser299), and phosphorylated signaling modules of the JNK and p38 MAPK pathways (supplemental Fig. S1, C1). Among them, the levels of p-p53 at Ser392, Ser37, and Ser6 differed substantially between groups A (low) and B (high) (supplemental Fig. S1). In addition, cell lines clustered into group A tended to have simultaneous phosphorylation of the mTOR signaling components C2, RPS6(Ser235/236), RPS6(Ser240/244), and eIF4G(Ser1108) (supplemental Fig. S1). With some notable exceptions, sorafenib-insensitive cell lines (high IC_{50} values for sorafenib) and sorafenib-sensitive cell lines (low IC_{50} values for sorafenib) were clustered into group A and group B, respectively. Although sorafenib-insensitive SNU-387, JHH-1, and KIM-1 cells were classified into the sorafenib-sensitive group B, their phosphorylation levels of mTOR signaling components C2 were higher than those in the other cell lines in group B, suggesting that activation of mTOR signaling might be responsible for the resistance to sorafenib in these cell lines. Some of the sorafenib-insensitive cell lines (*e.g.* Alexander, JHH-2, and SNU-475 cells) partitioned into subtype Ab (supplemental Fig. S1) were characterized by prominent activation of mTOR signaling components C2 and MAPK signaling components C1. Together, these findings imply that there is a certain population of HCC cells showing up-regulation of both mTOR and MAPK signaling. Such an HCC subtype might respond better to combination treatment with mTOR and MAPK inhibitors. When we compared the phosphorylation status of the mTOR and MAPK signaling nodes in 95 cell lines by means of unsupervised hierarchical clustering, HCC cell lines were significantly clustered together ($p = 0.011$ by Fisher's exact test) in group A (supplemental Fig. S2), characterized by high levels of phosphorylation of the signaling components C1 and C2, in comparison to cell lines derived from seven other cancer types (supplemental Table S10). The signaling components C1 included previously reported targets of sorafenib such as b-RAF and PDGF receptor-β, as well as the upstream modules of the mTOR pathway (*e.g.* Akt and PDK). The components C2 comprised RPS6(Ser235/236), RPS6(Ser240/244), eIF4G(Ser1108), and the signaling modules of the JNK and p38 MAPK pathways. These observations may reflect the fact that the activation of MAPK signaling by itself, or in combination with mTOR signaling, is a unique feature of HCC.

It is noteworthy that some sorafenib-sensitive and -insensitive cell lines were clustered together into subgroup Aa (supplemental Fig. S1). Although this subgroup was characterized by relatively low levels of both mTOR and MAPK signaling activation, the most sorafenib-sensitive cell line, SNU-449, was classified into this subgroup. It is therefore plausible that some other signaling pathway, in addition to the mTOR and MAPK pathways, may be involved in defining the marked sensitivity of SNU-449 cells to sorafenib.

DISCUSSION

Derangements in the phosphorylation of signaling molecules are hallmarks of cancers, and are often considered as targets of molecular therapies. By profiling the phosphorylation status of multiple signaling components, it is possible to derive important clues for understanding the pathogenesis and classification of cancers. In this study, a high level of p-RPS6 S235/236 was detected in sorafenib-resistant HCC cells. Consistent with this *in vitro* observation, such high expression of p-RPS6 S235/236 was detected in pretreatment biopsy specimens from HCC patients who had shown early radiographically evident disease progression after starting sorafenib therapy. The number of patient samples analyzed in this study was small and insufficient for providing conclusive evidence, but the present findings warrant future clinical studies to evaluate the significance of p-RPS6 S235/236 as a predictor of response to sorafenib. In order to ensure accurate validation of the utility of p-RPS6 S235/236 as a predictor in future studies, standardized guidelines of immunohistochemistry for detecting p-RPS6 (Ser235/236) need to be developed, including tissue preparation, fixation, staining methods, scoring system, and the definition of a "positive" result.

p-RPS6 has been used as a molecular surrogate for mTOR activation. Villanueva *et al.* (22) assessed 314 surgical specimens of HCC immunohistochemically using an anti-p-RPS6 S240/244 antibody. They detected p-RPS6 S240/244 in half of the cases examined, and positive staining was correlated with HCC recurrence (22). Although antibodies against p-RPS6 S235/236 and p-RPS6 S240/244 have been used equivalently in many studies to evaluate mTOR activation (22, 23), the phosphorylation of these serine residues was found to be differentially regulated (Fig. 2*A*). An earlier study demonstrated persistent phosphorylation of RPS6 S235/236 in cells derived from S6K1$^{-/-}$/S6K2$^{-/-}$ double-knockout mice, and it was concluded that this paradoxical phosphorylation was caused by MAPK signaling. A later study revealed that RSK (MAPK pathway) predominantly phosphorylated the serine 235 and 236 residues of RPS6, whereas S6K (mTOR pathway) broadly phosphorylated the serine 235, 236, 240, 244, and 247 residues. Therefore, use of an antibody against p-RPS6 S240/244 would seem more appropriate for specific detection of the mTOR pathway activation status (20). In the present study, however, we found that phosphorylation of the serine 235 and 236 residues of RPS6 reflected cross-talk between the mTOR and MAPK pathways (Fig. 3*C*) and served as a predictive biomarker of sorafenib sensitivity. Although RAF kinases (MAPK pathway) are one of the main molecular types targeted by sorafenib, intervention of active mTOR signaling in the MAPK pathway seems to be one of the molecular mechanisms responsible for the resistance of HCC to sorafenib.

It is therefore conceivable that HCC patients with tumors having high levels of p-RPS6 S235/236 could benefit from inhibition of mTOR signaling. We found that mTOR inhibitors showed greater antitumor activity against sorafenib-resisntant HCC cells (Fig. 3*E*). A recent phase I/II study of everolimus given daily as a single agent in patients with advanced HCC showed that the drug was well tolerated and exerted preliminary antitumor activity in some patients (24). A phase III EVOLVE-1 randomized trial is now ongoing to evaluate the efficacy of everolimus in HCC patients whose disease progressed during or after sorafenib treatment or who were intolerant to sorafenib (25). This clinical trial is designed to reveal the efficacy of mTOR pathway inhibition for control of sorafenib-resistant HCC and is expected to clarify the significance of our present findings.

Clustering analysis of RPPA data revealed that 6 out of 23 HCC cell lines (Alexander, JHH-2, SNU-475, Huh-7, KIM-1, and JHH-1) had prominent activation of both the MAPK and mTOR pathways, indicating a possible subset of HCC patients who might benefit from a combination of MAPK and mTOR inhibitors (supplemental Fig. S1). We also found synergy between MAPK and mTOR pathway inhibitors in sorafenib-resistant cell lines (Fig. 4). However, there is a need for caution before this can be applied clinically. Activation of MAPK signaling occurred at various levels of RAF/MEK/ERK/RSK in sorafenib-resistant cells (Fig. 3*C*). In addition, clustering analysis showed activation of two other major MAPK pathways, the Jun N-terminal kinase (JNK) and p38 MAPK pathways, in more than half the HCC cell lines (supplemental Fig. S1). Cross-talk among three major MAPK pathways (RAF/MEK/ERK, JNK, and p38MAPK) has been reported previously (26). Together, these findings suggest that careful assessment is vital when selecting an appropriate MAPK inhibitor for each individual HCC patient. Despite extensive sequencing of kinase genes, we were unable to identify any alterations in the pathway that might be responsible, indicating the need to expedite pharmacoproteomics for therapy personalization.

The present study highlighted the potential power of the RPPA platform for pathway profiling. We have provided proof-of-principle support for the utility of the highly sensitive, high-throughput RPPA platform by identifying a practical biomarker with potential clinical applicability. In this study, we used only well-characterized antibodies with high specificity. The Human Antibody Initiative is an ongoing project to raise at least one monospecific antibody against all >20,000 proteins encoded by the human genome (27). It is anticipated that the completion of this project will greatly accelerate the capability of RPPA. The majority of current molecular targeting drugs are designed to target a particular signaling pathway (28). Precise determination of signaling pathways that are activated in individual patients seems to be essential for obtaining maximum benefit from any given treatment. RPPA requires only a minuscule specimen quantity (*e.g.* less than 1 ng of protein per array) and is applicable even to small biopsy samples. The potential clinical utility of RPPA for decision-making and monitoring of cancer therapeutics is thus enormous.

* This work was supported by the National Cancer Center Research and Development Fund (23-A-38 and 23-A-11), the Program for Promotion of Fundamental Studies in Health Sciences conducted by the National Institute of Biomedical Innovation of Japan (10-07, 10-44, and 10-45), and the Research on Biological Markers for New Drug Development conducted by the Ministry of Health, Labor and Welfare of Japan.

[S] This article contains supplemental material.

§ To whom correspondence should be addressed: Mari Masuda, Ph.D., Division of Chemotherapy and Clinical Research, National Cancer Center Research Institute, Tokyo 104-0045, Japan, Tel.: 81-3-3542-2511 (ext. 4251), Fax: 81-3-3547-6045, E-mail: mamasuda@ncc.go.jp.

REFERENCES

1. Ferlay, J., Shin, H. R., Bray, F., Forman, D., Mathers, C., and Parkin, D. M. (2010) Estimates of worldwide burden of cancer in 2008: GLOBOCAN 2008. *Int. J. Cancer* **127,** 2893–2917
2. Llovet, J. M., Ricci, S., Mazzaferro, V., Hilgard, P., Gane, E., Blanc, J. F., de Oliveira, A. C., Santoro, A., Raoul, J. L., Forner, A., Schwartz, M., Porta, C., Zeuzem, S., Bolondi, L., Greten, T. F., Galle, P. R., Seitz, J. F., Borbath, I., Haussinger, D., Giannaris, T., Shan, M., Moscovici, M., Voliotis, D., and Bruix, J. (2008) Sorafenib in advanced hepatocellular carcinoma. *N. Engl. J. Med.* **359,** 378–390
3. Arao, T., Ueshima, K., Matsumoto, K., Nagai, T., Kimura, H., Hagiwara, S., Sakurai, T., Haji, S., Kanazawa, A., Hidaka, H., Iso, Y., Kubota, K.,

Shimada, M., Utsunomiya, T., Hirooka, M., Hiasa, Y., Toyoki, Y., Hakamada, K., Yasui, K., Kumada, T., Toyoda, H., Sato, S., Hisai, H., Kuzuya, T., Tsuchiya, K., Izumi, N., Arii, S., Nishio, K., and Kudo, M. (2013) FGF3/FGF4 amplification and multiple lung metastases in responders to sorafenib in hepatocellular carcinoma. *Hepatology* **57,** 1407–1415

4. Cheng, A. L., Kang, Y. K., Chen, Z., Tsao, C. J., Qin, S., Kim, J. S., Luo, R., Feng, J., Ye, S., Yang, T. S., Xu, J., Sun, Y., Liang, H., Liu, J., Wang, J., Tak, W. Y., Pan, H., Burock, K., Zou, J., Voliotis, D., and Guan, Z. (2009) Efficacy and safety of sorafenib in patients in the Asia-Pacific region with advanced hepatocellular carcinoma: a phase III randomised, double-blind, placebo-controlled trial. *Lancet Oncol.* **10,** 25–34
5. Wilhelm, S. M., Adnane, L., Newell, P., Villanueva, A., Llovet, J. M., and Lynch, M. (2008) Preclinical overview of sorafenib, a multikinase inhibitor that targets both Raf and VEGF and PDGF receptor tyrosine kinase signaling. *Mol. Cancer Ther.* **7,** 3129–3140
6. Abou-Alfa, G. K., Schwartz, L., Ricci, S., Amadori, D., Santoro, A., Figer, A., De Greve, J., Douillard, J. Y., Lathia, C., Schwartz, B., Taylor, I., Moscovici, M., and Saltz, L. B. (2006) Phase II study of sorafenib in patients with advanced hepatocellular carcinoma. *J. Clin. Oncol.* **24,** 4293–4300
7. Ueshima, K., Kudo, M., Takita, M., Nagai, T., Tatsumi, C., Ueda, T., Kitai, S., Ishikawa, E., Yada, N., Inoue, T., Hagiwara, S., Minami, Y., Chung, H., and Sakurai, T. (2011) Des-gamma-carboxyprothrombin may be a promising biomarker to determine the therapeutic efficacy of sorafenib for hepatocellular carcinoma. *Dig. Dis.* **29,** 321–325
8. Hagiwara, S., Kudo, M., Nagai, T., Inoue, T., Ueshima, K., Nishida, N., Watanabe, T., and Sakurai, T. (2012) Activation of JNK and high expression level of CD133 predict a poor response to sorafenib in hepatocellular carcinoma. *Br. J. Cancer* **106,** 1997–2003
9. Nishizuka, S., Charboneau, L., Young, L., Major, S., Reinhold, W. C., Waltham, M., Kouros-Mehr, H., Bussey, K. J., Lee, J. K., Espina, V., Munson, P. J., Petricoin, E., 3rd, Liotta, L. A., and Weinstein, J. N. (2003) Proteomic profiling of the NCI-60 cancer cell lines using new high-density reverse-phase lysate microarrays. *Proc. Natl. Acad. Sci. U.S.A.* **100,** 14229–14234
10. Byers, L. A., Wang, J., Nilsson, M. B., Fujimoto, J., Saintigny, P., Yordy, J., Giri, U., Peyton, M., Fan, Y. H., Diao, L., Masrorpour, F., Shen, L., Liu, W., Duchemann, B., Tumula, P., Bhardwaj, V., Welsh, J., Weber, S., Glisson, B. S., Kalhor, N., Wistuba, I. I., Girard, L., Lippman, S. M., Mills, G. B., Coombes, K. R., Weinstein, J. N., Minna, J. D., and Heymach, J. V. (2012) Proteomic profiling identifies dysregulated pathways in small cell lung cancer and novel therapeutic targets including PARP1. *Cancer Discov.* **2,** 798–811
11. Spurrier, B., Ramalingam, S., and Nishizuka, S. (2008) Reverse-phase protein lysate microarrays for cell signaling analysis. *Nat. Protoc.* **3,** 1796–1808
12. Bolstad, B. M., Irizarry, R. A., Astrand, M., and Speed, T. P. (2003) A comparison of normalization methods for high density oligonucleotide array data based on variance and bias. *Bioinformatics* **19,** 185–193
13. Masuda, M., Maruyama, T., Ohta, T., Ito, A., Hayashi, T., Tsukasaki, K., Kamihira, S., Yamaoka, S., Hoshino, H., Yoshida, T., Watanabe, T., Stanbridge, E. J., and Murakami, Y. (2010) CADM1 interacts with Tiam1 and promotes invasive phenotype of human T-cell leukemia virus type I-transformed cells and adult T-cell leukemia cells. *J. Biol. Chem.* **285,** 15511–15522
14. Li, H., and Durbin, R. (2009) Fast and accurate short read alignment with Burrows-Wheeler transform. *Bioinformatics* **25,** 1754–1760
15. Li, H., Handsaker, B., Wysoker, A., Fennell, T., Ruan, J., Homer, N., Marth, G., Abecasis, G., Durbin, R., and Genome Project Data Processing, S. (2009) The Sequence Alignment/Map format and SAMtools. *Bioinformatics* **25,** 2078–2079
16. Wang, K., Li, M. Y., and Hakonarson, H. (2010) ANNOVAR: functional annotation of genetic variants from high-throughput sequencing data. *Nucleic Acids Res.* 38(16):e164.
17. Chou, T. C. (2010) Drug combination studies and their synergy quantification using the Chou-Talalay method. *Cancer Res.* **70,** 440–446
18. Anjum, R., and Blenis, J. (2008) The RSK family of kinases: emerging roles in cellular signalling. *Nat. Rev. Mol. Cell Biol.* **9,** 747–758
19. Pende, M., Um, S. H., Mieulet, V., Sticker, M., Goss, V. L., Mestan, J., Mueller, M., Fumagalli, S., Kozma, S. C., and Thomas, G. (2004) S6K1(−/−)/S6K2(−/−) mice exhibit perinatal lethality and rapamycin-sensitive 5′-terminal oligopyrimidine mRNA translation and reveal a mitogen-activated protein kinase-dependent S6 kinase pathway. *Mol. Cell. Biol.* **24,** 3112–3124
20. Roux, P. P., Shahbazian, D., Vu, H., Holz, M. K., Cohen, M. S., Taunton, J., Sonenberg, N., and Blenis, J. (2007) RAS/ERK signaling promotes site-specific ribosomal protein S6 phosphorylation via RSK and stimulates cap-dependent translation. *J. Biol. Chem.* **282,** 14056–14064
21. Ascierto, P. A., Kirkwood, J. M., Grob, J. J., Simeone, E., Grimaldi, A. M., Maio, M., Palmieri, G., Testori, A., Marincola, F. M., and Mozzillo, N. (2012) The role of BRAF V600 mutation in melanoma. *J. Transl. Med.* **10,** 85
22. Villanueva, A., Chiang, D. Y., Newell, P., Peix, J., Thung, S., Alsinet, C., Tovar, V., Roayaie, S., Minguez, B., Sole, M., Battiston, C., Van Laarhoven, S., Fiel, M. I., Di Feo, A., Hoshida, Y., Yea, S., Toffanin, S., Ramos, A., Martignetti, J. A., Mazzaferro, V., Bruix, J., Waxman, S., Schwartz, M., Meyerson, M., Friedman, S. L., and Llovet, J. M. (2008) Pivotal role of mTOR signaling in hepatocellular carcinoma. *Gastroenterology* **135,** 1972–1983
23. Zhou, L., Huang, Y., Li, J., and Wang, Z. (2010) The mTOR pathway is associated with the poor prognosis of human hepatocellular carcinoma. *Med. Oncol.* **27,** 255–261
24. Zhu, A. X., Abrams, T. A., Miksad, R., Blaszkowsky, L. S., Meyerhardt, J. A., Zheng, H., Muzikansky, A., Clark, J. W., Kwak, E. L., Schrag, D., Jors, K. R., Fuchs, C. S., Iafrate, A. J., Borger, D. R., and Ryan, D. P. (2011) Phase 1/2 study of everolimus in advanced hepatocellular carcinoma. *Cancer* **117,** 5094–5102
25. Kudo, M. (2011) Signaling pathway and molecular-targeted therapy for hepatocellular carcinoma. *Dig. Dis.* **29,** 289–302
26. Wagner, E. F., and Nebreda, A. R. (2009) Signal integration by JNK and p38 MAPK pathways in cancer development. *Nat. Rev. Cancer* **9,** 537–549
27. Uhlen, M., and Ponten, F. (2005) Antibody-based proteomics for human tissue profiling. *Mol. Cell. Proteomics* **4,** 384–393
28. Wulfkuhle, J. D., Edmiston, K. H., Liotta, L. A., and Petricoin, E. F., 3rd (2006) Technology insight: pharmacoproteomics for cancer—promises of patient-tailored medicine using protein microarrays. *Nat. Clin. Pract. Oncol.* **3,** 256–268

Supplementary Figure Legends

Figure S1. Unsupervised hierarchical clustering of the 23 HCC cell lines (horizontal axis) and phosphorylation status of the mTOR and MAPK signaling nodes (vertical axis). Red, white and blue colors indicate high, intermediate and low levels of signaling node phophorylation. Light green and yellow represent signaling components of the MAPK pathway and mTOR pathway, respectively. Signaling components of the MAPK and mTOR pathways highly related to HCC cell line subtypes are labeled C1 and C2, respectively. Clustering revealed formation of 2 major groups, A and B, in the cell lines. The 10 cell lines that showed the highest IC50 for sorafenib are highlighted in orange.

Figure S2. Unsupervised hierarchical clustering of the 95 HCC cell lines (horizontal axis) and phosphorylation status of the mTOR and MAPK signaling nodes (vertical axis). Red, white and blue colors indicate high, intermediate and low levels of signaling node phophorylation. Light green and yellow represent signaling components of the MAPK pathway and mTOR pathway, respectively. Signaling components related to HCC cell line subtypes are labeled C1 and C2, respectively. Clustering revealed formation of 2 major groups, A and B, in the cell lines. The 23 HCC cell lines are highlighted in purple.